Avoided-crossing molecular-beam spectroscopy of symmetric tops. I. Phosphoryl fluoride (OPF_3)

IRVING OZIER[1]

Fysisch Laboratorium, Katholieke Universiteit, Toernooiveld, Nijmegen, The Netherlands, and Department of Physics, University of British Columbia, Vancouver, B.C., Canada V6T 1W5

AND

W. LEO MEERTS

Fysisch Laboratorium, Katholieke Universiteit, Toernooiveld, Nijmegen, The Netherlands

Received May 20, 1980

A new avoided-crossing technique using a conventional molecular beam electric resonance spectrometer has been developed for studying symmetric rotors. By means of an external electric field, two levels with different values of K are made nearly degenerate and normally forbidden electric-dipole transitions between the interacting levels are observed. Mixing matrix elements η_{ST} with $\Delta K = \pm 3$ arise from the centrifugal distortion dipole moment μ_D and mixing terms η_{HYP} with $\Delta K = \pm 1, \pm 2$ arise from the nuclear hyperfine Hamiltonian. Explicit expressions for η_{HYP} are given in an Appendix. Many of these terms break the symmetry of both the rotational and nuclear spin parts of the wave functions. The avoided-crossing method is discussed in detail, with emphasis on its application to the measurement of $(A_0 - B_0)$. It is shown how the technique can be used to determine the perpendicular moment μ_D, as well as μ_J and μ_K, the constants which characterize the dependence of the parallel dipole moment μ on J and K, respectively. Other applications include the experimental investigation of the selection rules for the individual terms in η_{HYP} and the determination of the sign of the rotational g-factors $g_{\|}$ and $g_{\perp}$. The method has been applied to phosphoryl fluoride (OPF_3). It has been determined that $(A_0 - B_0) = 217.4987(44)$ MHz, $\mu_D = 5.856(20) \times 10^{-6}$ D, $\mu_J = -3.38(10) \times 10^{-6}$ D, and both $g_{\|}$ and $g_{\perp}$ are negative.

On a développé une nouvelle technique de croisements évités utilisant un spectromètre conventionnel à résonance électrique de faisceau moléculaire pour l'étude de rotateurs symétriques. Au moyen d'un champ électrique extérieur deux niveaux ayant des valeurs différentes de K sont rendus presque dégénérés, et l'interaction entre les niveaux permet d'observer des transitions de dipôle électrique normalement défendues. Des éléments de matrice η_{ST} avec $\Delta K = \pm 3$ proviennent du moment dipolaire de distortion centrifuge μ_D, et des termes de mélange η_{HYP} avec $\Delta K = \pm 1, \pm 2$ proviennent de l'hamiltonien de structure hyperfine. Des expressions explicites pour η_{HYP} sont données en Appendice. Plusieurs de ces termes brisent la symétrie de la partie rotationnelle et de la partie spin nucléaire des fonctions d'onde. On discute de façon détaillée la méthode des croisements évités, en insistant particulièrement sur son application à la mesure de $(A_0 - B_0)$. On montre comment la technique peut être utilisée pour déterminer le moment perpendiculaire μ_D aussi bien que μ_J et μ_K, les constantes qui caractérisent la façon dont le moment de dipôle dépend de J et K respectivement. Parmi les autres applictions, il y a l'étude expérimentale des règles de sélection pour les termes individuels dans η_{HYP} et la détermination du signe des facteurs g rotationnels, $g_{\|}$ et $g_{\perp}$. La méthode a été appliquée au fluorure de phosphoryle (OPF_3). On a déterminé que $(A_0 - B_0) = 217{,}4987(44)$ MHz, $\mu_D = 5{,}856(20) \times 10^{-6}$ D, $\mu_J = -3{,}38(10) \times 10^{-6}$ D, et que $g_{\|}$ et $g_{\perp}$ sont tous deux négatifs.

[Traduit par le journal]

Can. J. Phys., **59**, 150 (1981)

1. Introduction

Symmetry properties often make important molecular parameters inaccessible to the spectroscopist. For a polar symmetric top, the normal electric dipole moment $\boldsymbol{\mu}$ lies along the symmetry axis. This leads directly to the well-known ($\Delta K = 0$) selection rule for electric dipole transitions within the ground vibronic state and thereby makes it impossible to apply conventional microwave methods to the measurement of A_0, a constant of prime importance in the determination of molecular structures. In the current work, a simple avoided-crossing technique (1)[2] based on the molecular beam electric resonance (mber) method is described in which the ($\Delta K = 0$) selection rule is broken along with other selection rules dealing with the conservation of the symmetry of the rotational and nuclear spin parts of the wave function. No other technique for observing radiative

[1]Permanent address: Department of Physics, University of British Columbia, Vancouver, B.C., V6T 1W5.

[2]A preliminary report of part of this work was given in ref. 1.

0008-4204/81/010150-22$01.00/0

transitions resulting from such symmetry breaking has been previously developed for symmetric rotors.

In addition to providing a precision value for A_0, this anticrossing method can be used to investigate a series of other interesting molecular problems. First, the effects of centrifugal distortion on the electric dipole operator can be studied in detail. These effects generate a small moment μ_D perpendicular to the axis (2, 3) and cause the magnitude of the parallel moment to become a function of J and K. For matrix elements diagonal in J, this function takes the form (4)

$$[1] \qquad \mu(J, K) = \mu_0 + \mu_J J(J+1) + \mu_K K^2$$

where μ_0 is the equilibrium moment (except for a small correction), while μ_J and μ_K are distortion dipole constants.[3] In favorable cases, μ_J, μ_K, and μ_D can all be determined by the current technique in spite of the fact that each is typically five to six orders of magnitude smaller than μ_0. Second, the nuclear hyperfine interactions can be investigated. Measurements of the terms diagonal in $|K|$ can act as a useful complement to results obtainable with previous methods. Perhaps more important, the terms off-diagonal in $|K|$ can be studied; terms of this type are inaccessible to conventional spectroscopy. These off-diagonal matrix elements can provide an important mechanism for the relaxation of interstellar molecules (6). Third, the sign of the rotational g-factor can be determined. This sign is often difficult to obtain, since many of the standard methods (7) of studying g-factors yield only the magnitude. These different applications of the anticrossing method are discussed here with respect to phosphoryl fluoride (OPF_3). In a later work, the application recently introduced (8) of the method to the study of internal rotation will be treated in detail.

The essential features of the technique can be explained in terms of a simple two level problem. Consider a pair of levels in the isolated molecule in field-free space with different K values such that the state of higher energy $E_0(K_\alpha)$ has a negative Stark effect and that of lower energy $E_0(K_\beta)$ has a positive Stark effect. Such a situation is illustrated in Fig. 1 where $K_\alpha = \pm 2$ and $K_\beta = \mp 1$.[4] Here $E_0(\pm 2) > E_0(\mp 1)$ because OPF_3 is a prolate rotor. The molecular is placed in a homogeneous external electric field $\mathscr{E}$ which is increased until the difference

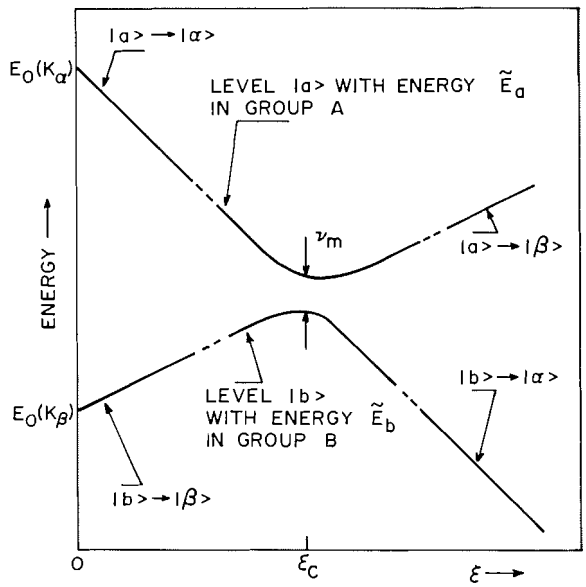

FIG. 1. Schematic plot against electric field of the energies of two anticrossing levels. The breaks in the energy levels allow the central region to be plotted on a different scale where both coordinates are greatly expanded. As an example of the general problem illustrated here, $|a\rangle \to |J_\alpha = 2,\ K_\alpha = \pm 2, m_J^\alpha = \pm 2, m_{P^\alpha} = +\frac{1}{2},\ m_F^\alpha = +\frac{1}{2}\rangle$ and $|b\rangle \to |J_\beta = 2, K_\beta = \mp 1, m_J^\beta = \pm 2,\ m_{P^\alpha} = +\frac{1}{2}, m_F^\alpha = +\frac{1}{2}\rangle$. Each level is labelled by its high field quantum numbers for $\mathscr{E} \ll \mathscr{E}_C$.

Δ_{ST} in the Stark energies exactly cancels the difference $\Delta_0 \equiv [E_0(K_\alpha) - E_0(K_\beta)]$ in the zero field energies. At this particular field, termed the "crossing" field $\mathscr{E}_C$, the two levels will undergo an avoided crossing provided there is a non-zero coupling matrix element η. At $\mathscr{E} = \mathscr{E}_C$, the two levels have their minimum separation $\nu_m = 2|\eta|$. There are two types of avoided crossings: *Stark* anticrossings in which η arises from the interaction of μ_D and $\mathscr{E}$, and *hyperfine* anticrossings in which η arises from nuclear hyperfine interactions.

The two principal parameters, $\mathscr{E}_C$ and ν_m, that characterize the anticrossing can be measured with a conventional mber spectrometer. For values of $\mathscr{E}$ near $\mathscr{E}_C$, the two interacting levels are thoroughly mixed and transitions between them are easily driven through μ by applying an oscillating electric field $\mathscr{E}_{RF}$. To lowest order, $\mathscr{E}_C$ is proportional to Δ_0/μ. If a magnetic field B is applied in addition to $\mathscr{E}$, then $\mathscr{E}_C$ is still defined by the condition that the energy difference in the absence of mixing vanishes, but now the Zeeman contribution must be taken into account. In this case, $\mathscr{E}_C$ is a function of Δ_0, μ, and $g_{eff}B$, where g_{eff} is the effective g-factor for the anticrossing.

Recently, a number of related studies of $^{16}OPF_3$

[3] In order to conform to the conventions adopted by other authors, e.g., ref. 5, the signs of μ_J and μ_K here have been reversed relative to those used in ref. 1.

[4] Unless otherwise specified, it will be assumed throughout that upper signs go with upper signs and lower with lower.

TABLE 1. Molecular constants for OPF_3 in the ground vibronic state

Quantity	Value	Reference
B_0 (MHz)	4594.2624(5)	10
$(A_0 - B_0)$ (MHz)	217.4987(44)[a]	Present work
	217.4954(18)	11
	217.54(5)	12
D_J (kHz)	1.0119(12)	10, 11[b]
D_{JK} (kHz)	1.2971(7)	11
D_K (kHz)	−1.114(12)	11
μ_0 (D)[c,d]	1.86847(10)	9
μ_D (D)[c]	$5.856(20)\times10^{-6}$	Present work
μ_J (D)[c]	$-3.38(10)\times10^{-6}$ [a]	Present work
$g_\perp$ (nm)	−0.04460(4)	9, present work[e]
$g_\parallel$ (nm)	−0.03370(30)	9, present work[e]

[a]There is a small difference from the value given in the preliminary report in ref. 1 because minor refinements were made in the analysis.
[b]This value was obtained in ref. 11 by reanalysing the data in ref. 10.
[c]The magnitudes of μ_0, μ_J, and μ_D were determined along with the relative sign of μ_J and μ_0 (see footnote 3).
[d]This is actually μ_r as obtained from the allowed transition ($J_K = 3_{\pm2}, m_J = \mp1 \rightarrow 0$) selected as reference, but $|\mu_0 - \mu_r|$ is negligible compared to the absolute error.
[e]The magnitudes and relative sign of $g_\perp$ and $g_\parallel$ were determined in ref. 9. The absolute sign was established in the present work.

in the ground vibronic state have been carried out. Some of the results are summarized in Table 1. A detailed conventional mber experiment (9) has been completed, giving a precision value for μ_0, many of the nuclear hyperfine constants, and the magnitudes of the rotational g-factors. Both the "normal" mm spectrum (10) driven by μ with selection rules $\Delta J = +1$, $\Delta K = 0$ and the "forbidden" microwave spectrum (11)[5] driven by μ_D with selection rules $\Delta J = 0$, $\Delta K = \pm3$ have been observed. An analysis (11) of the combined data set yielded B_0, A_0, the three quartic distortion constants D_J, D_{JK}, and D_K, and the four sextic distortion constants. Most recently, laser Stark spectroscopy (12) has been used to observe anticrossings of the Stark type to give a value for $(A_0 - B_0)$. Much of the theoretical analysis developed here for the mber experiments may ultimately find application in such laser-Stark studies. The conventional mber method (9), the mm-wave spectroscopy (10), and the laser Stark methods (13) have all been applied to various excited vibrational states.

In the following section, the theoretical aspects of the current method are discussed. In Sect. 2*A*, the high-field representation used to calculate the Hamiltonian matrix in the crossing region is described and, in Sect. 2*B*, the two level problem is solved in detail. The Stark anticrossings are then discussed in Sect. 2*C*. The coupling selection rules and matrix elements are given, the focussing problem is treated, the lowest crossing fields are calculated, and the detailed form of the spectrum is derived. The different applications and their accuracy limitations are discussed. Finally, the two-level assumption is justified. In Sect. 2*D*, a similar treatment of the hyperfine anticrossings is presented. In this case, the coupling matrix elements are more complicated and are presented in the Appendix. Magnetic effects receive more attention. The general use of the lowest crossing field of the $(\Delta J = 0)$ type for measuring $(A_0 - B_0)$ is discussed.

In Sect. 3, the experimental aspects of the method are treated with emphasis on the C-field. The ultimate limitation on the highest $(A_0 - B_0)$ that can be measured for a given μ is discussed. In Sect. 4, the results for OPF_3 are given and, in Sect. 5, a brief discussion is presented comparing the current technique to some of the other methods of measuring A_0.

2. Theory

A. The High Field Energies

The effective Hamiltonian for a symmetric top in external electric and magnetic fields can be written as:

$$[2] \qquad H = H_{ROT} + H_{ST} + H_Z + H_{HYP}$$

H_{ROT} is the rotational Hamiltonian. H_{ST} and H_Z are, respectively, the interactions with $\mathscr{E}$ and B, which are parallel in the current work. H_{HYP} is the nuclear hyperfine contribution. In OPF_3 with the two magnetic nuclei P and F, this is made up of two spin–rotation interactions, $H_{IJ}{}^P$ and $H_{IJ}{}^F$, and two spin–spin interactions, $H_{II}{}^{PF}$ and $H_{II}{}^{FF}$. In typical high-field mber spectroscopy, the energies corresponding to the four terms in [2] form the hierarchy $|E_{ROT}| \gg |E_{ST}| \gg |E_Z| \gtrsim |E_{HYP}|$.

The space-fixed coordinate system is oriented with $\hat{Z}$ along the common direction of $\mathscr{E}$ and B. The molecule-fixed coordinate system is oriented with $\hat{z}$ along the symmetry axis. The fluorine nuclei are numbered 1, 2, and 3 in a clockwise direction as one looks in the positive z direction; nucleus No. 1 is in the yz plane, which consequently is one of the σ_v planes of the molecule. This orientation is illustrated in Fig. 3*a* of Wofsy *et al.* (14).

The high-field representation (9, 14) used here is characterized by the quantum numbers $(J,K,m_J; I_P,m_P;I_F,m_F)$. The fluorine nuclear spin $I_F = 3/2$ or $1/2$ corresponding, respectively, to $K = 3N$ (N an integer) and $K \neq 3N$. m_J, m_P, and m_F are, respectively, the eigenvalues of the Z-component of $\boldsymbol{J}$, $\boldsymbol{I}_P$, and $\boldsymbol{I}_F$. The sum $m_T = m_J + m_P + m_F$ is the eigenvalue of the Z-component of the total angular

[5]The preliminary avoided-crossing molecular-beam work in ref. 1 and microwave work in ref. 11 were carried out concurrently.

momentum. The basis functions in this representation are discussed in the Appendix.

This high-field representation forms the zeroth order basis for calculating the Hamiltonian matrix in the anticrossing regions. It is therefore necessary to define clearly the conditions under which the off-diagonal matrix elements of H can be neglected. First, $\mathscr{E}$ is assumed to be large enough that the matrix elements of H_{HYP} with ($\Delta K = 0$, $\Delta m_J \neq 0$) can be dropped. Second, $\mathscr{E}$ is assumed to be far enough from any crossing field that the coupling η off-diagonal in K can be neglected. Finally, B is taken to be >2 mT to lift certain degeneracies as described below. The only significant off-diagonal matrix elements remaining are those due to μ and these have *only* $\Delta J \neq 0$.[6]

Under these conditions, the high field energy E_α for state $|\alpha\rangle$ is calculated by two different methods. In the first, E_{ST} is calculated by perturbation theory, while the diagonal matrix elements are used for the other three terms in [2]. A second-order treatment of H_{ST} is very instructive and will be outlined here. A third-order treatment (9) is required for preliminary analysis. To obtain the accuracy required for the final results, the second method is used. The full matrix $H_{\mathrm{ROT}} + H_{\mathrm{ST}}$ is diagonalized after truncation at $\Delta J \leq 3$. H_Z and H_{HYP} are still treated in the original high-field representation.

The rotational energy, in SI units, is given by

$$[3] \qquad E_{\mathrm{ROT}}/h = B_0 J(J+1) + (A_0 - B_0)K^2 - D_J J^2(J+1)^2 - D_{JK} J(J+1)K^2 - D_K K^4$$

The fundamental constants given in ref. 15 are used. The molecular constants are in Hz. The sextic distortion contribution is negligible.

The Stark energy is given by:

$$[4] \qquad E_{\mathrm{ST}} = \frac{-\mu \mathscr{E} m_J K}{J(J+1)} + \frac{\mu^2 \mathscr{E}^2}{2hB_0} F(J, K, m_J)$$

To second order in $\mathscr{E}$, the function F depends only on the quantum numbers and can be deduced from Gordy and Cook (16). In general, however, F will include all the necessary higher order terms and will be a function of $\mu\mathscr{E}/B_0$ as well. The dipole constants μ_0, μ_J, and μ_K in [1] can be related to the distortion-dipole coefficients $\Theta_\alpha^{\beta\gamma}$ defined by Watson *et al.* (4)[7]

$$[5a] \qquad \mu_0 = \mu_z^{(e)} - \Theta_y^{yz}$$

$$[5b] \qquad \mu_J = \Theta_z^{yy} + 2\Theta_z^{yz}$$

$$[5c] \qquad \mu_K = \Theta_z^{zz} - (\Theta_z^{yy} + 2\Theta_y^{yz})$$

Here $\mu_z^{(e)}$ is the equilibrium electric dipole moment. Effects due to the anisotropy ($\alpha_\parallel - \alpha_\perp$) in the polarizability can be neglected.

The Zeeman energy can be written:

$$[6] \qquad E_Z = -(1-\sigma_P)g_P m_P \mu_N B - (1-\sigma_F)g_F m_F \mu_N B - [g_\perp + (g_\parallel - g_\perp)K^2/J(J+1)]m_J \mu_N B$$

For nucleus λ = P or F, g_λ and σ_λ are the g-factor and average magnetic shielding, respectively. $g_\parallel$ and $g_\perp$ are, respectively, the molecular g-factor for rotation parallel and perpendicular to the symmetry axis. The anisotropies in the shielding and the terms quadratic in B are negligible here.

The hyperfine energy E_{HYP} is given in [2] of Meerts *et al.* (9). The same notation is used here. The spin rotation constants that enter are $c_\perp^{\mathrm{P}}$, $c_\parallel^{\mathrm{P}}$, $c_\perp^{\mathrm{F}}$, and $c_\parallel^{\mathrm{F}}$. In this case, the subscript $\perp$ means an average is to be taken about the x and y axes. The spin–spin constants that enter E_{HYP} are d^{FF} and d^{PF} for the fluorine–fluorine and fluorine–phosphorus interactions, respectively. These are defined in [A8].

The condition that $B > 2$ mT as assumed in setting up the high-field representation allows us to neglect two types of off-diagonal elements due to H_{II}^{PF}.[6] To abbreviate the notation, these are represented here by $D_{|\Delta K|}^{\mathrm{PF}}(K_L)$, where K_L is the algebraically lower of the two K values. The first type arises from terms for which $\Delta J = \Delta K = \Delta m_J = 0$ and $\Delta m_P = -\Delta m_F = \pm 1$ (see [4] in Table IV of Wofsy *et al.* (14)). These terms D_0^{PF} are proportional to d^{PF}. They connect levels degenerate with respect to H_{ST}. For $B = 0$, the diagonal terms only in H_{HYP} are available to split the levels. A detailed analysis of the hyperfine problem is then required to see if m_F and m_P are good quantum numbers. However, the diagonal elements $\langle H_Z \rangle$ will separate these levels; for $B > 2$ mT, the mixing due to D_0^{PF} can be neglected.

[6] If $|K| = 1$ and $m_J = 0$, K is not a good quantum number for any $\mathscr{E}$ or B because of the K-doubling term in H_{II}^{PF} which can be obtained from [1E] of Table IV in ref. 14. See also [A6] in the Appendix here. For this special case, the high-field states are not $|K = +1, m_J = 0\rangle$ and $|-1,0\rangle$, but rather $(1/\sqrt{2})\{|+1,0\rangle \pm |-1,0\rangle\}$. The treatment of the avoided crossings can be modified to take this complication into account. The major conclusions are similar, but some of the detailed arguments are different. However, because none of the anticrossings studied experimentally in OPF_3 involve states of this type, the necessary modifications are not presented.

[7] The coordinate system used in ref. 4 is not the same as that used here and in several other works, e.g., ref. 14, involving nuclear hyperfine structure. To convert [5] and [14] to the coordinate system in ref. 4, the labels on the Θ's and τ must be changed as follows: $z \to \zeta$, $y \to \xi$, and $x \to \eta$. A similar transformation is required to convert to the coordinate system of ref. 2.

The second type of troublesome H_{II}^{PF} matrix element arises from K-doubling terms for which $\Delta J = 0, \Delta K = \pm 2, \Delta m_J = \mp 2, \Delta m_P = \pm 1, \Delta m_F = \pm 1$ (see [A6] here and [5E] in Table IV of ref. 14). These terms D_2^{PF} are proportional to $\frac{1}{2}(d_{xx}^{PF} - d_{yy}^{PF})$ as defined in [A8]. For $(K,m_J) = (\pm 1,\pm 1)$ or $(\pm 1, \mp 1)$, the levels connected by D_2^{PF} are degenerate with respect to both H_{ST} and the diagonal terms in H_{HYP}. As a result, the entire representation breaks down for the connected levels if $B = 0$. Again $\langle H_Z \rangle$ lifts the degeneracy and, for $B \gtrsim 2$ mT, the mixing due to D_2^{PF} can be neglected. If $K \neq \pm 1$ or $m_J \neq \pm 1$, the levels mixed by D_2^{PF} have different values of $\langle H_{ST} \rangle$ and the D_2^{PF} matrix elements have no significant effect. There are K-doubling terms (14) due to the fluorine spin–rotation interaction arising from $\frac{1}{2}(c_{xx}^F - c_{yy}^F)$, but these cannot couple $m_J = \pm 1$ to $m_J' = \mp 1$ and so do not connect degenerate levels even when $B = 0$. Thus in a conventional mber problem in large electric fields,[6] only the one K-doubling term, namely D_2^{PF}, connects levels degenerate in H_{ST} and its effects can be reduced to a second-order perturbation correction by applying a small magnetic field. The two terms D_0^{PF} and D_2^{PF}, will be discussed further when the anticrossings are treated.

B. The Two Level Problem

Each anticrossing system such as that illustrated in Fig. 1 involves two groups of levels, A and B. The letters are selected so that A has the higher energy. Each group is labelled by its (J,K,m_J) for $\mathscr{E} \ll \mathscr{E}_C$. Because $(E_{ROT} + E_{ST})$ is the same for (J,K,m_J) as for $(J,-K,-m_J)$, this group label is "sign doubled," e.g., $(2,\pm 2,\pm 2)$, except when $K = m_J = 0$. Each level within a group has its own m_P and m_F, as well as a specific sign (upper or lower) in the group label. The anticrossing system is specified by the group labels for A and B.

In spite of the multiplicity of levels within each group, it is assumed in this section that the anticrossing system can be treated as a series of independent problems, each involving only two levels, one from A and one from B. In later sections, the two level assumption will be discussed in detail.

The high-field basis functions used to calculate the two-dimensional Hamiltonian matrix are represented by $|\alpha\rangle$ and $|\beta\rangle$. The high-field energies calculated as described in Sect. 2*A* are E_α and E_β. The sets of high-field quantum numbers α and β are selected so that $E_\alpha > E_\beta$ for $\mathscr{E} < \mathscr{E}_C$. Thus, far below $\mathscr{E}_C$, α and β specify single levels in groups A and B, respectively (see Fig. 1).

In this truncated basis, the effective Hamiltonian matrix is

$$[7] \qquad (H)_{\alpha\beta} = \begin{pmatrix} E_\alpha & \eta \\ \eta^* & E_\beta \end{pmatrix}$$

The eigenfunctions are referred to as $|a\rangle$ and $|b\rangle$ corresponding to eigenvalues $\tilde{E}_a$ and $\tilde{E}_b$, respectively, where $\tilde{E}_a > \tilde{E}_b$. Clearly a is a single level in group A and b is its partner in group B. The tildes are introduced to indicate explicitly the distinction between the eigenvalues, which are the energies with the coupling η turned on, and the diagonal matrix elements, which are the energies with η turned off.

The physical properties of $|a\rangle$ and $|b\rangle$ are interchanged as $\mathscr{E}$ is increased through $\mathscr{E}_C$, as can be seen in Fig. 1, for example. Well below $\mathscr{E}_C$, $|a\rangle$ behaves as almost pure $|\alpha\rangle = |J = 2, K = \pm 2, m_J = \pm 2\rangle$ and has a negative Stark effect, while $|b\rangle$ behaves as almost pure $|\beta\rangle = |J = 2, K = \mp 1, m_J = \pm 2\rangle$ and has a positive Stark effect. Well above $\mathscr{E}_C$, the two Stark effects have been interchanged and the K values have been switched: $|a\rangle \rightarrow |\beta\rangle = |K = \mp 1\rangle$ and $|b\rangle \rightarrow |\alpha\rangle = |K = \pm 2\rangle$. At $\mathscr{E} = \mathscr{E}_C$, $|a\rangle$ is an equal mixture of $|\alpha\rangle$ and $|\beta\rangle$; $|b\rangle$ is also completely mixed, but is, as always, orthogonal to $|a\rangle$.

The transition frequency between the two interacting levels is

$$[8] \qquad \nu = [(E_\alpha - E_\beta)^2 + 4|\eta|^2]^{1/2}$$

The difference in the diagonal elements can be written

$$[9a] \qquad E_\alpha - E_\beta = \Delta_{ROT} + \Delta_{ST} + \Delta_Z + \Delta_{HYP}$$

where each Δ is the indicated difference in the high-field energies. The difference Δ_0 introduced in Sect. 1 equals the field-independent terms $(\Delta_{ROT} + \Delta_{HYP})$. The crossing field is defined by the condition

$$[9b] \qquad E_\alpha - E_\beta = 0 \text{ at } \mathscr{E} = \mathscr{E}_C$$

It is often convenient to approximate [8] by

$$[10] \qquad \nu \doteqdot [(\mathscr{E} - \mathscr{E}_C)^2 s_C^2 + 4|\eta|^2]^{1/2}$$

where $s_C = (\partial\Delta_{ST}/\partial\mathscr{E})$ evaluated at $\mathscr{E} = \mathscr{E}_C$. This approximation is valid for the interval in $\mathscr{E}$ about $\mathscr{E}_C$ for which the derivative s can be considered to be constant. The value of s_C can be calculated accurately from the known value of μ and even a very approximate measurement of $\mathscr{E}_C$. For the typical η encountered here, [10] can be used out to values of $\nu \gg |\eta|$. If $|\eta|$ is negligible in [10], then ν becomes a linear function of $\mathscr{E}$:

$$[11] \qquad \nu \doteqdot |(\mathscr{E} - \mathscr{E}_C)s_C|$$

The best way of measuring $\mathscr{E}_C$ and η is to follow ν right through the anticrossing region. The values

obtained will be uncorrelated. $\mathscr{E}_C$ will be determined by measurements in the linear region where $\nu \gg |\eta|$ and $|\eta|$ will be determined by measurements near $\mathscr{E}_C$ where ν reaches its minimum value $\nu_m = 2|\eta|$. In many cases, however, this "right-through" method is not practical and only a crude estimate or upper limit for $|\eta|$ can be obtained. In these cases, an uncorrelated value of $\mathscr{E}_C$ can be determined by first establishing the range in $\mathscr{E}$ for which [11] is valid and then making a single measurement in this range. This "one-sided" method, of course, uses the known value of s_C. Alternatively, ν is measured at a field far enough below $\mathscr{E}_C$ that $|\partial\nu/\partial\mathscr{E}|$ is a sizable fraction of $|s_C|$. A second measurement is then made at the same frequency but with $\mathscr{E}$ above $\mathscr{E}_C$. As long as the two frequencies in this "above/below" method are approximately equal, $\mathscr{E}_C$ can be found by linear interpolation without using s_C or $|\eta|$.

In order to induce transitions between $|a\rangle$ and $|b\rangle$, an oscillating electric field of amplitude $\mathscr{E}_{RF}$ is applied. Since $\Delta m_T = 0$, $\mathscr{E}_{RF}$ is applied parallel to $\mathscr{E}$. The transition operator $V = -\boldsymbol{\mu}\cdot\mathscr{E}_{RF}$ acts through the normal moment and the mixing of the high-field states. The magnitude of the transition matrix element is given by

$$[12] \qquad |\langle a|V|b\rangle| = \left|\frac{\eta}{\nu}\mu\mathscr{E}_{RF}\left\{\frac{m_J{}^{\alpha}K_\alpha}{J_\alpha(J_\alpha+1)} - \frac{m_J{}^{\beta}K_\beta}{J_\beta(J_\beta+1)}\right\}\right|$$

This result applies right through the crossing region, in spite of the fact that it is expressed in terms of the limiting high-field quantum numbers. In order to make the transition probability unity for a beam of velocity v, $|\langle a|V|b\rangle| = hv/2L$, where L is the length of the transition region (17, 18). For the Stark crossing shown in Fig. 1 and $|\eta/\nu| = 10^{-3}$, the optimum $\mathscr{E}_{RF}$ is 4.7 V/cm, a value which is easily attained, particularly at low frequencies $\lesssim$10 MHz.

Under the two level assumption, each anticrossing system $(J_\alpha K_\alpha m_J{}^{\alpha}) \leftrightarrow (J_\beta K_\beta m_J{}^{\beta})$ will yield at each $\mathscr{E}$ near its $\mathscr{E}_C$ a spectrum consisting of a series of lines, one for each pair of interacting levels. Thus there are two lines for each $(m_P{}^{\alpha}, m_F{}^{\alpha}) \leftrightarrow (m_P{}^{\beta}, m_F{}^{\beta})$, one for each sign in the sign-doubled group level. The lines in this series will come at different frequencies because $\mathscr{E}_C$ will depend on the sign choice and on the values of m_P and m_F through Δ_Z and Δ_{HYP}. If $\mathscr{E}$ is fixed far enough below $\mathscr{E}_C$ that [11] applies for *all* members of the series, then, because s_C is the same for all members, the lines fall in the same order and with the same separation as they would in the limit $\mathscr{E} \to 0$. This is referred to as the *normal* spectrum. If $\mathscr{E}$ is fixed at a value which is a similar increment above $\mathscr{E}_C$, the order of the lines is reversed, but the spacings are preserved. This is referred to as the *inverted* spectrum. In order to deduce the form of these spectra, the selection rules, the coupling η, and the crossing field $\mathscr{E}_C$ must be calculated.

C. Stark Anticrossings

The mixing in this case between the high field states $|\alpha\rangle$ and $|\beta\rangle$ is done by the Stark effect due to $\mu_D{:}\eta_{ST} = \langle\alpha|(-\mu_Z'\mathscr{E})|\beta\rangle$ where μ_Z' is the space-fixed Z component of the distortion dipole operator given in [8] of ref. 2. For η_{ST} to be non-zero, $|\alpha\rangle$ and $|\beta\rangle$ must satisfy the selection rules (2) $\Delta J = (J_\alpha - J_\beta) = 0, \pm1$; $\Delta K = (K_\alpha - K_\beta) = \pm3$. The K-selection rule implies that $\Delta I_F = 0$; the symmetries of the rotational and nuclear spin parts of the wave function are individually conserved. Because the Stark operator does not affect the nuclear spin variables, $\Delta m_P = \Delta m_F = 0$. Since $\Delta m_T = 0$ for any anticrossing, it follows that $\Delta m_J = 0$ as well. For $(\alpha = J,K+3,m_J,m_P,m_F) \leftrightarrow (\beta = J,K,m_J,m_P,m_F)$ (2),[8]

$$[13] \quad \eta_{ST}{}^{Q}(J,K,m_J) = \tfrac{1}{2}i\mu_D\mathscr{E}[m_J/J(J+1)] \times [(J-K)(J-K-1)(J-K-2) \times (J+K+1)(J+K+2)(J+K+3)]^{1/2}$$

The distortion dipole moment is defined[7] by (2, 3):

$$[14a] \quad \mu_D = \Theta_y{}^{yy} + \Theta_{ROT}$$

where $\Theta_y{}^{yy}$ and Θ_{ROT} are the vibrational and rotational terms, respectively. Θ_{ROT} can be related to the centrifugal distortion constant τ_{yyyz}:

$$[14b] \quad \Theta_{ROT} = -\hbar^4\tau_{yyyz}\mu_0/2h(A_0 - B_0)$$

For $(\alpha = J-1,K+3,m_J,m_P,m_F) \leftrightarrow (\beta = J,K,m_J,m_P,m_F)$ (2),[8]

$$[15] \quad \eta_{ST}{}^{P}(J,K,m_J) = \tfrac{1}{2}i\mu_D\mathscr{E} \times [(J^2 - m_J{}^2)/J^2(4J^2-1)]^{1/2} \times [(J-K)(J-K-1)(J-K-2) \times (J-K-3)(J+K+1)(J+K+2)]^{1/2}$$

A similar expression can be derived for $\eta_{ST}{}^{R}(J,K,m_J)$ for the crossing $(J+1,K+3,m_J,m_P,m_F) \leftrightarrow (J,K,m_J,m_P,m_F)$.

In order for the anticrossing $|\alpha\rangle \leftrightarrow |\beta\rangle$ to be detected by an mber spectrometer, the states $|\alpha\rangle$

[8] Since by definition $E_\alpha > E_\beta$ for $\mathscr{E} \ll \mathscr{E}_C$, it has been assumed here implicitly that $E(J',K+3,m_J) > E(J,K,m_J)$ for $\mathscr{E} \ll \mathscr{E}_C$. If this assumption is incorrect, the identifications of α and β must be interchanged and i must be replaced by i^*.

and $|\beta\rangle$ must satisfy conditions imposed by the focussing properties of the quadrupole deflection fields. Since $E_\alpha > E_\beta$ for $\mathscr{E} < \mathscr{E}_C$, these conditions are met for the standard "flop-out" quadrupole configuration (17, 19) if $|\beta\rangle$ is a focussed state ($\partial E_\beta/\partial\mathscr{E} > 0$) and $|\alpha\rangle$ is defocussed ($\partial E_\alpha/\partial\mathscr{E} < 0$) or poorly focussed ($\partial E_\alpha/\partial\mathscr{E} > 0$, but small).

In practice, there are three different cases in which these conditions are met. In case I, $|\beta\rangle$ and $|\alpha\rangle$ have, respectively, positive and negative linear Stark effects. This requires that $(K_\beta m_J{}^\beta)$ and $(K_\alpha m_J{}^\alpha)$ have opposite signs. Since $\Delta m_J = 0$, K must change sign in the transition. This can happen only for $(K_\alpha = \pm 2) \leftrightarrow (K_\beta = \mp 1)$. Case I can occur in oblate and prolate tops for both $\Delta J = 0$ and ± 1. In case II, $|\beta\rangle$ and $|\alpha\rangle$ have, respectively, positive quadratic and negative linear Stark effects. This can happen only for $K_\beta = 0$ and $K_\alpha = \pm 3$. Case II can occur in a prolate rotor for $\Delta J = 0$ and ± 1, but in an oblate rotor only for $\Delta J = \pm 1$. In case III, $|\beta\rangle$ and $|\alpha\rangle$ have, respectively, positive linear and negative quadratic Stark effects. Here $K_\beta = \pm 3$ and $K_\alpha = 0$. Case III can occur in an oblate top for $\Delta J = 0$ and ± 1, but in a prolate top only for $\Delta J = \pm 1$. Thus Stark crossings can be detected directly only for $K = \pm 2 \leftrightarrow \mp 1$ and $K = \pm 3 \leftrightarrow 0$.[9] Other changes in K can be detected, but generally require significant additional innovation, such as the introduction of double resonance.

In considering the feasibility of an anticrossing experiment, one of the first questions that must be answered is whether the lowest $\mathscr{E}_C$ for the molecule can be attained in the laboratory. An approximate value of $\mathscr{E}_C$ can be obtained from [9] by taking into account only the rigid rotor part of Δ_{ROT} along with the linear terms in Δ_{ST}. Both Δ_{HYP} and Δ_Z are neglected. For $(J,K+3,m_J) \leftrightarrow (J,K,m_J)$ in a prolate top,

$$[16] \qquad \mathscr{E}_C = \left| \frac{h(A_0 - B_0)(2K+3)}{\mu} \frac{J(J+1)}{m_J} \right|$$

This equation applies to an oblate rotor if $(A_0 - B_0)$ is replaced by $(B_0 - C_0)$. Many anticrossings of this type with different J and m_J can occur for fields of the same order of magnitude. The lowest set of $\mathscr{E}_C$ values arises for $K = \pm 2 \leftrightarrow \mp 1$, with the second lowest set coming from $K = \pm 3 \leftrightarrow 0$. Some overlap exists between the field regions for the different sets. Fortunately, these two families are the very ones which meet the focussing conditions. The lowest $\mathscr{E}_C$ for a $(\Delta J = 0)$ anticrossing system arises for $(J,K,m_J) = (2, \pm 2, \pm 2) \leftrightarrow (2, \mp 1, \pm 2)$.

For $\Delta J = \mp 1$ in a prolate top, the lowest crossing fields occur for $\Delta K = \pm 3$. For $(J-1, K+3, m_J) \leftrightarrow (J,K,m_J)$,

$$[17] \qquad \mathscr{E}_C = \left| \frac{h\{3(A_0 - B_0)(2K+3) - 2B_0 J\}}{(2K+3J+3)\mu} \times \frac{(J-1)J(J+1)}{m_J} \right|$$

Note that $|K+3| \leq (J-1)$. In order for $\mathscr{E}_C$ to be attainable here, there is usually a nearly complete cancellation between two large terms in Δ_{ROT}, one in $(A_0 - B_0)$ and the other in B_0. As a result, $\mathscr{E}_C$ is low only for one or two specific J_K. This cancellation takes place if A_0/B_0 is close to $(2J + 6K + 9)/(6K + 9)$. For example, if $A_0/B_0 = 11/3$, $J_K = 4_{\mp 1}$ is degenerate with $3_{\pm 2}$ and $\mathscr{E}_C \to 0$. Similar results apply to the oblate rotor, except that the lowest values of $\mathscr{E}_C$ occur for $\Delta J = \pm 1$, $\Delta K = \pm 3$.

To predict the shape and average frequency of the *normal* spectrum of an anticrossing system for given $\mathscr{E}$ and B, the value of $\mathscr{E}_C$ for each interacting pair in the system must be calculated in full. All the Stark anticrossings investigated to date are of the type $(J,K_\alpha = \pm 2, m_J) \leftrightarrow (J,K_\beta = \mp 1, m_J)$. The discussion here will be confined to this case, but it can be extended to other anticrossings in a straightforward manner. In order to obtain $\mathscr{E}_C$ from [9], the dipole moment is treated in Δ_{ST} as a constant equal to the value μ_r for an allowed transition such as $(J_r,K_r,m_J{}^r = \mp 1 \to 0)$ which has been selected as reference. The effect of the variation of μ with J and K is absorbed into Δ_{ROT} to form an apparent $\Delta_{ROT}{}^A$. The only significant difference between $\Delta_{ROT}{}^A$ and Δ_{ROT} is the contribution of μ_J and μ_K entering through the linear Stark effect. The value of $\mathscr{E}_C$ is then given by:

$$[18a] \qquad \frac{3\mu_r \mathscr{E}_C m_J}{J(J+1)} - \frac{\mu_r{}^2 \mathscr{E}_C{}^2}{2hB_0}[F(J,\pm 2, m_J) - F(J,\mp 1, m_J)] = \Delta_{ROT}{}^A + \Delta_Z + \Delta_{HYP}$$

where

$$[18b] \qquad \Delta_{ROT}{}^A = 3a - 3J(J+1)b$$

$$[18c] \qquad a = (A_0 - B_0)[1 + \varepsilon] - 5D_K$$

$$[18d] \qquad b = D_{JK} + (A_0 - B_0)\mu_J/\mu_0$$

$$[18e] \qquad \varepsilon = J_r(J_r+1)(\mu_J/\mu_0) + (K_r{}^2 - 3)(\mu_K/\mu_0)$$

$$[18f] \qquad \Delta_Z = -3(g_\parallel - g_\perp)\mu_N B m_J/J(J+1)$$

$$[18g] \qquad \Delta_{HYP} = 3(c_\parallel{}^P - c_\perp{}^P)m_P m_J/J(J+1) + 3(c_\parallel{}^F - c_\perp{}^F)m_F m_J/J(J+1) - 18d^{PF}\left\{\frac{3m_J{}^2 - J(J+1)}{(2J-1)(2J+3)}\right\} \times m_P m_F/J(J+1)$$

[9] When a crossing is referred to without specifying which level is $|\alpha\rangle$ and which is $|\beta\rangle$, the quantum number(s) for $|\alpha\rangle$ will be given first.

In these equations, m_J will be positive for $K_\alpha = +2$ and negative for $K_\alpha = -2$. The function F superficially has the form of the second order Stark effect and can be so interpreted in qualitative work. However, as indicated in Sect. 2*A*, F includes all the higher order terms required by the experimental accuracy; one must be careful *not* to absorb any of these terms into $\Delta_{ROT}{}^{A}$.

The essential features of the shape of the *normal* spectrum can be determined directly from the right-hand side of [18] because the coupling η is the same for each interacting pair in the anticrossing system. The spectrum will consist of two magnetic components whose g-factors are equal in magnitude and opposite in sign. For positive $(g_\parallel - g_\perp)$, the high and low frequency components will correspond to $-|m_J|$ and $+|m_J|$ respectively. Each component has the same fine structure due to Δ_{HYP}. This is symmetric about the $(\Delta_{HYP} = 0)$ position. For the OPF_3 coupling constants given in Table 1 of ref. 8 and the full width at half-height of the instrumental line shape $\Delta\nu$ of 18 kHz, this fine structure in the individual components cannot be resolved. The splitting $2|\Delta_Z|$ between components is symmetric about the $(B = 0)$ position and can be resolved at the highest B. However, for $B \lesssim 0.1$ T, the splitting cannot be resolved. In this case, the spectrum of the entire anticrossing system will consist of a single line symmetric about the $(\Delta_Z + \Delta_{HYP} = 0)$ position.

The frequency of this single line at given $\mathscr{E}$ can be calculated from [11] using $\mathscr{E}_C$ obtained from [18*a*] with only $\Delta_{ROT}{}^{A}$ taken into account on the right-hand side. It follows then that $\mathscr{E}_C$ for a Stark anticrossing system is independent of magnetic and hyperfine effects. This type of anticrossing is consequently ideally suited to precision studies of E_{ROT} and E_{ST}. By measuring $\Delta_{ROT}{}^{A}$ for a series of different J, the two constants a and b can be determined.

The accuracy possible in measuring $\Delta_{ROT}{}^{A}$ must be given careful consideration because $|b/a|$ is generally very small, $\sim 5 \times 10^{-6}$ in OPF_3. The anticrossing frequencies can usually be measured to sufficient accuracy that the error is dominated by the contributions from μ_r and the field calibration. Since $\mathscr{E}$ is the ratio of the voltage V applied across the C-field plates to their separation d, $\Delta_{ROT}{}^{A}$ can be expressed as a function of the crossing voltage V_C multiplied by (μ_r/d). By using conventional mber spectroscopy to study the reference allowed transition, (μ_r/d) can be reduced to the ratio of a frequency to a second voltage measurement multiplied by a frequency ratio (see Sect. 3). Since typically the frequency errors can all be made negligible, the uncertainty in $\Delta_{ROT}{}^{A}$ is determined by the total error in a single voltage ratio. The fractional error in this ratio is limited to $\sim 2 \times 10^{-5}$ by the absolute long term stability of the voltage source. Thus a can be obtained to $\sim 0.002\%$. If μ_r and d are measured separately using the most accurate means possible, this error would be over twice as large. However, $bJ(J+1)$ is still the order of the error in a, so that a determination of b to good accuracy, e.g., 1%, can generally not be made by a series of independent measurements for the comparatively low J's accessible.

To overcome this difficulty, *relative* measurements are made. Two anticrossing systems with different J but nearly equal $\mathscr{E}_C$ are selected and $\mathscr{E}$ is set at a value such that [11] applies to all lines in each spectrum. By observing both spectra in the same field, the *difference* in the two values of $\Delta_{ROT}{}^{A}$ is obtained to an accuracy determined by the short term stability of the voltage source, namely 2×10^{-6}. If, in addition, the two anticrossing systems have the same linear coefficient in Δ_{ST}, then the difference in the two Δ_{ST} depends only on the quadratic (and higher) contributions and the difference in the two $\Delta_{ROT}{}^{A}$ will depend only on the term in b. Thus the fractional contribution due to b is greatly increased and accuracy $\sim 1\%$ can be obtained. Two such anticrossings are $(J = 2, m_J = \pm 1, K = \pm 2 \leftrightarrow \mp 1)$ and $(J = 5, m_J = \pm 5, K = \pm 2 \leftrightarrow \mp 1)$. The effect of field inhomogeneities on the accuracy is discussed in Sect. 3.

The separation of b into its two terms in [18] is generally not difficult because D_{JK} can usually be obtained to sufficient accuracy by conventional mm-wave spectroscopy. This yields a value for μ_J. The separation of a in [18] is somewhat more difficult. Three independent pieces of information are needed to obtain $(A_0 - B_0)$, μ_K, and D_K. If D_K is available from the distortion moment spectrum, as is the case for OPF_3 (11), then relative measurements involving the $(K = \pm 2 \leftrightarrow \mp 1)$ series and the $(K = \pm 3 \leftrightarrow 0)$ series of anticrossings will provide the remaining two constants. Otherwise, a third series of anticrossings is necessary. However, both the term in μ_K and that in D_K are typically $\lesssim 2 \times 10^{-5}$ of $(A_0 - B_0)$, leading to an absolute contribution which is just the order of the absolute experimental error in a. As a result, the final accuracy in $(A_0 - B_0)$ is generally not seriously degraded if a separation of a into its different terms is not possible.

The entire analysis to this point has been based on the *two-level assumption*. Because of the high precision required for many of the applications, it is necessary to show in some detail that this assumption is valid. The system $A \equiv (J, K_\alpha = \pm 2, m_J{}^{\alpha} = \pm 2) \leftrightarrow B \equiv (J, K_\beta = \mp 1, m_J{}^{\beta} = \pm 2)$ is selected as an example. There are eight levels in group A and eight in group B. The states with $m_J = +2$ cannot couple to those with $m_J = -2$ because no interaction available can satisfy a selection rule with $|\Delta m_J| > 2$.

Each group of eight levels then splits into two subgroups of four. We consider here only the levels with $m_J = +2$. The levels with $m_J = -2$ can be treated by identical arguments. Because m_T is a good quantum number, the four levels in B with $(J,K_\beta = -1,m_J{}^\beta = +2)$ break up into three blocks, one for each possible value of m_T: $(m_J{}^\beta - 1) = +1$, $m_J{}^\beta = 2$, and $(m_J{}^\beta + 1) = 3$. For $m_T = +1$, there is a unique set of values possible for the nuclear magnetic quantum numbers: $m_P{}^\beta = -\frac{1}{2}$, $m_F{}^\beta = -\frac{1}{2}$. This can couple with only one level in group A, namely $(J,K_\alpha = +2,m_J{}^\alpha = +2,m_P{}^\alpha = -\frac{1}{2},m_F{}^\alpha = -\frac{1}{2})$, and a 2×2 problem results. Similarly, for $m_T = +3$, there is a single combination (m_P,m_F) available in B and in A, so that the two-level assumption is again valid.

However, for $m_T = m_J = 2$, there are two possible combinations (m_P,m_F) available in β: $\beta 1 \rightarrow (-\frac{1}{2},+\frac{1}{2})$ and $\beta 2 \rightarrow (+\frac{1}{2},-\frac{1}{2})$. These two can interact with each other by means of the phosphorus–fluorine spin–spin terms $D_0{}^{PF}(-1)$ introduced in Sect. 2*A*. There is a similar situation in A: $\alpha 1 \rightarrow (-\frac{1}{2},+\frac{1}{2})$ and $\alpha 2 \rightarrow (+\frac{1}{2},-\frac{1}{2})$ interact through $D_0{}^{PF}(+2)$. The anticrossing problem then involves a 4×4 Hamiltonian matrix of the form shown in Table 2. If $D_0{}^{PF}$ could be neglected, this (4×4) matrix would reduce to two independent (2×2) blocks.

In order for this reduction to occur, two ratios must be negligible: $|D_0{}^{PF}(-1)/[E_{\beta 1} - E_{\beta 2}]|$ and $|D_0{}^{PF}(+2)/[E_{\alpha 1} - E_{\alpha 2}]|$. For $B \gtrsim 2$ mT, the nuclear Zeeman contribution to the energy denominators will generally make both of these ratios very small. For lower values of B, a detailed calculation must be done whose results depend on the specific molecule's coupling constants. In OPF_3, the energy denominators are large compared to $|D_0{}^{PF}|$ all the way down to $B = 0$, where the denominators arise primarily from $H_{IJ}{}^P$ and $H_{IJ}{}^F$. As a result, the $(m_T = +2)$ case can be broken up into two separate two dimensional problems. Furthermore, it can be shown that the $(\Delta_Z + \Delta_{HYP})$ contribution to $\mathscr{E}_C$ in [18] is negligible even for $B < 2$ mT.

From these arguments, it is clear that the two level analysis presented can be applied to any Stark anticrossing system with $|m_J| \geq 2$. For $|m_J| = 1$, the situation is more complicated because the separation of $+m_J$ from $-m_J$ does not occur in such a simple manner. In fact, for $|m_J| = 1$, the system is not truly Stark in nature, but is a *hybrid* of Stark and hyperfine mixing. Such systems are discussed in Sect. 2*D*.

D. Hyperfine Anticrossings

For the hyperfine avoided crossings, the two-level assumption will again be adopted initially and subsequently examined in depth. The mixing between the high field states $|\alpha\rangle$ and $|\beta\rangle$ by H_{HYP} has been analysed in detail. The matrix elements are given in the Appendix. The different interactions, the coupling constants, and the selection rules are summarized in Table 3.

Since $\Delta K = \pm 1$ and ± 2 are allowed for the coupling η_{HYP}, avoided crossings occur in which $(K = 3N) \leftrightarrow (K \neq 3N)$. In such anticrossings, $\Delta I_F = \pm 1$; the symmetries of both the rotational and nuclear spin parts of the wave function are individually broken. This breaking of the molecular symmetry by some of the interactions can be understood on simple physical grounds. The rotational magnetic field at the phosphorus clearly had C_{3v} symmetry; this leads directly to the absence of $(\Delta K \neq 0)$ terms in $H_{IJ}{}^P$. On the other hand, the rotational magnetic field seen by an individual fluorine nucleus clearly does not have C_{3v} symmetry and is therefore able to produce $(\Delta K \neq 0)$ terms in $H_{IJ}{}^F$. This rotational field is inhomogeneous across the fluorine nucleus, as it must be to change I_F.

Similar arguments can be made for $H_{II}{}^{PF}$ and $H_{II}{}^{FF}$, with one notable difference. An operator of the form $H_{II}{}^{FF}$ with $(\Delta K = \pm 1)$ matrix elements can be formed according to group theory, but the coupling constant $\frac{1}{2}(d_{yz}{}^{FF} + d_{zy}{}^{FF}) \equiv 0$ for the classical spin–spin mechanism because the three fluorine nuclei are all in a plane perpendicular to the z-axis. The forces involved in the electron-coupled spin–spin mechanism are not symmetric about this plane. These would produce a non-zero $(\Delta K = \pm 1)$ term of the $H_{II}{}^{FF}$ form, but the coupling constant would be extremely small because the fluorine atoms are not directly bonded to each other.

The two $(\Delta K = \pm 1)$ coupling constants enter conventional spectroscopy only in second-order perturbation theory and consequently have not been measured for any symmetric top. For a rigid molecule, the $(\Delta K = \pm 2)$ constant $\frac{1}{2}(d_{xx}{}^{FF} - d_{yy}{}^{FF})$ is proportional to the $(\Delta K = 0)$ constant d^{FF} (see [A8]) and so can be determined by conventional mber experiments (9). All three $(\Delta K = \pm 2)$ constants can have a K-doubling contribution to the energy for $K = \pm 1$, but the measurement of these terms is difficult and has been done only for very few molecules such as NH_3 (20). The classical spin–spin constants can, of course, be calculated from the molecular structure (see the Appendix).

The focussing requirements for the hyperfine anticrossings are very similar to those for the Stark anticrossings, with the same three cases possible. In case I, $(K_\beta m_J{}^\beta)$ and $(K_\alpha m_J{}^\alpha)$ can have opposite signs now only for $m_J = \pm 1 \leftrightarrow \mp 1$. This can occur in oblate and prolate tops for both $\Delta J = 0$ and ± 1. In case II, K_β and/or m_β must vanish and, in case III, K_α and/or m_α must vanish. Because of the many

TABLE 2. The Hamiltonian matrix with $m_T = m_J$ for the Stark anticrossing problem $(J,K = +2 \leftrightarrow -1, m_J = +2 \leftrightarrow +2)$[a]

K,m_J,m_P,m_F	$-1,+2,-\frac{1}{2},+\frac{1}{2}$	$+2,+2,-\frac{1}{2},+\frac{1}{2}$	$-1,+2,+\frac{1}{2},-\frac{1}{2}$	$+2,+2,+\frac{1}{2},-\frac{1}{2}$
$-1,+2,-\frac{1}{2},+\frac{1}{2}$	$E_{\beta 1}$	η_{ST}	$D_0^{PF}(-1)$	0
$+2,+2,-\frac{1}{2},+\frac{1}{2}$	η_{ST}^*	$E_{\alpha 1}$	0	$D_0^{PF}(+2)$
$-1,+2,+\frac{1}{2},-\frac{1}{2}$	$D_0^{PF}(-1)^*$	0	$E_{\beta 2}$	η_{ST}
$+2,+2,+\frac{1}{2},-\frac{1}{2}$	0	$D_0^{PF}(+2)^*$	η_{ST}^*	$E_{\alpha 2}$

[a] D_0^{PF} is the matrix element of H_{II}^{PF}. Since $\Delta K = 0$, the argument in parentheses equals either K-value.

TABLE 3. The interactions, coupling constants, and selection rules[a] for the hyperfine interactions

Interaction	ΔJ	Δm_J	Δm_P	Δm_F	Coupling constant[b] for: $\Delta K = 0$	$\Delta K = \pm 1$	$\Delta K = \pm 2$
H_{IJ}^F	$0,\pm 1$	$0,\pm 1$	0	$0,\mp 1$	$c_a^{F\,c}$ $\frac{1}{3}(c_\parallel^F - c_\perp^F)$	$\frac{1}{2}(c_{yz}^F + c_{zy}^F)$	$\frac{1}{2}(c_{xx}^F - c_{yy}^F)$
H_{IJ}^P	$0,\pm 1$	$0,\pm 1$	$0,\mp 1$	0	$c_a^{P\,c}$ $\frac{1}{3}(c_\parallel^P - c_\perp^P)$	0	0
H_{II}^{PF}	$0,\pm 1,\pm 2$	$0,\pm 1,\pm 2$	$0,\mp 1$	$0,\mp 1$	d^{PF}	$\frac{1}{2}(d_{yz}^{PF} + d_{zy}^{PF})$	$\frac{1}{2}(d_{xx}^{PF} - d_{yy}^{PF})$
H_{II}^{FF}	$0,\pm 1,\pm 2$	$0,\pm 1,\pm 2$	0	$0,\mp 1,\mp 2$	d^{FF}	0	$\frac{1}{2}(d_{xx}^{FF} - d_{yy}^{FF})$

[a] The values from the Δm_J, Δm_P, and Δm_F columns must be selected so that $\Delta m_T = 0$.
[b] See the Appendix for definition of the spin–spin constants in terms of molecular parameters and the resulting numerical values for OPF_3.
[c] $c_a^\lambda \equiv \frac{1}{3}(2c_\perp^\lambda + c_\parallel^\lambda)$ where $\lambda = P$ or F.

different selection rules, a complete breakdown of the different anticrossings detectable in these two cases is too lengthy to be given here, but the problem is straightforward.

The detailed form of the *normal* spectrum of a hyperfine anticrossing system is very similar to that for Stark anticrossings, but has several important differences, many of which can be traced to the fact that the magnetic quantum numbers now can change. In this discussion, it is very helpful to use a specific system as an example. The anticrossing systems studied here in OPF_3 are listed in Table 4. In each case, the coupling constants capable of providing the required mixing are given. The example chosen is $(1,\pm 1,\pm 1) \leftrightarrow (1,0,0)$. Both $\frac{1}{2}(c_{yz}^F + c_{zy}^F)$ and $\frac{1}{2}(d_{yz}^{PF} + d_{zy}^{PF})$ fit selection rules (*i*) $\Delta m_J = \pm 1$, $\Delta m_P = 0$, $\Delta m_F = \mp 1$, but only $\frac{1}{2}(d_{yz}^{PF} + d_{zy}^{PF})$ fits selection rules (*ii*) $\Delta m_J = \pm 1$, $\Delta m_P = \mp 1$, $\Delta m_F = 0$. The analogue of [18] forms the basis for calculating the spectrum. The result is not given here, but can be obtained by the reader from Sect. 2*A*.

In describing the essential features of the resulting spectrum, it is initially assumed that only selection rules (*ii*) are operative. The normal spectrum will then consist of one pair of magnetic components. Unlike the Stark case, each line within a given component will have a different η because the mixing depends now on (m_P,m_F). In spite of this, the two components have the same fine structure: for each line in the first component there is a corresponding line in the second with the same η and the same shift due to Δ_{HYP}. The distribution of frequencies within each component is not symmetric about the ($\Delta_{HYP} = 0$) position. The fine structure cannot be resolved in OPF_3 with the current instrumental line width $\Delta\nu$.

For any specific line within a magnetic component of a hyperfine system with $\Delta J = (J_\alpha - J_\beta) = 0$, the effective g-factor, defined as $-(\partial\Delta_Z/\partial B)$ in nuclear magnetons, is given by:

$$[19] \quad g_{eff} = +(1-\sigma_P)g_P\Delta m_P + (1-\sigma_F)g_F\Delta m_F + g_\perp\Delta m_J + (g_\parallel - g_\perp)[K_\alpha{}^2 m_J{}^\alpha - K_\beta{}^2 m_J{}^\beta]/J(J+1)$$

For the selection rules now being considered in the example, ($\Delta m_J = +1$, $\Delta m_P = -1$, $\Delta m_F = 0$) will produce the high-frequency component, since g_P is positive. A sign reversal for all three Δm's will produce the low-frequency component. The two g-factors have the same magnitudes but opposite signs. Because of the large nuclear contribution to g_{eff}, the two components are easily resolved even for B as small as 2 mT. It is often convenient to approximate g_{eff} by these dominant nuclear terms:

$$[20] \quad \tilde{g} = +g_P\Delta m_P + g_F\Delta m_F$$

For both members of this particular magnetic pair, $|\tilde{g}| = g_P$. The specification of $|\tilde{g}|$ in terms of g_P and g_F provides a convenient method of giving the selection rules on Δm_P and Δm_F.

In studying this spectrum, the variation of $|\langle a|V|b\rangle|$ with ν indicated in [12] must be taken into account. If $\mathscr{E}_{RF}/\nu$ is held approximately constant for both components and all B, then the spectrum takes

TABLE 4. The hyperfine anticrossings observed: the mixing mechanisms and splitting patterns

J	$K_\alpha \leftrightarrow K_\beta$	$m_J^\alpha \leftrightarrow m_J^\beta$	Coupling constant allowed	$\lvert\tilde{g}\rvert$ [a]	n	Observed[b] relative intensity per component
1	$\pm1 \leftrightarrow 0$	$\pm1 \leftrightarrow 0$	$\frac{1}{2}(c_{yz}^{F} + c_{zy}^{F})$ $\frac{1}{2}(d_{yz}^{PF} + d_{zy}^{PF})$	g_F g_F	3	4
				g_P	2	4
2	$\pm1 \leftrightarrow 0$	$\pm1 \leftrightarrow 0$	$\frac{1}{2}(c_{yz}^{F} + c_{zy}^{F})$ $\frac{1}{2}(d_{yz}^{PF} + d_{zy}^{PF})$	g_F g_F	3	4
				g_P*	2	2.7[c]
2	$\pm2 \leftrightarrow 0$	$\pm2 \leftrightarrow \pm1$	$\frac{1}{2}(c_{xx}^{F} - c_{yy}^{F})$ $\frac{1}{2}(d_{xx}^{FF} - d_{yy}^{FF})$ $\frac{1}{2}(d_{xx}^{PF} - d_{yy}^{PF})$	g_F g_F g_F	4	3
				g_P*	2	1.5[c]
2	$\pm1 \leftrightarrow 0$	$\pm2 \leftrightarrow 0$	$\frac{1}{2}(d_{yz}^{PF} + d_{zy}^{PF})$	$g_P + g_F$	2	8
2	$\pm2 \leftrightarrow 0$	$\pm2 \leftrightarrow 0$	$\frac{1}{2}(d_{xx}^{FF} - d_{yy}^{FF})$	$2g_F$	2	25
			$\frac{1}{2}(d_{xx}^{PF} - d_{yy}^{PF})$	$g_P + g_F$	2	25
2[d]	$\pm2 \leftrightarrow \pm1$	$\pm1 \leftrightarrow \mp1$	$\frac{1}{2}(d_{yz}^{PF} + d_{zy}^{PF})$	$g_P + g_F$	1	140
3[d]	$\pm2 \leftrightarrow \pm1$	$\pm1 \leftrightarrow \mp1$	$\frac{1}{2}(d_{yz}^{PF} + d_{zy}^{PF})$	$g_P + g_F$	1	35[b]
3	$\pm3 \leftrightarrow \pm2$	$\pm1 \leftrightarrow \mp1$	$\frac{1}{2}(d_{yz}^{PF} + d_{zy}^{PF})$	$g_P + g_F$	2	4

[a] All the predicted magnetic components were observed experimentally except the two marked with an asterisk.
[b] For comparison, on this intensity scale, the pure Stark component of the $(J = 3, K = \pm2 \leftrightarrow \mp1, m_J = \pm1 \leftrightarrow \pm1)$ hybrid system has strength 250.
[c] These intensities were calculated using the n ratios from the intensities observed for $|\tilde{g}| = g_F$.
[d] This refers only to the $(m_T = 0)$ hyperfine satellites in the hybrid Stark-hyperfine system.

its simplest form. The shapes of the two components are identical and do not change with B. Their shifts from their $(\Delta_{HYP} = 0)$ positions are similarly equal and independent of B. The splitting is symmetric about the $(B = 0)$ position and varies according to a g-factor whose magnitude is $|2g_{eff}|$.

In the actual spectrum, selection rules (i) are also operative. This set of selection rules has $|\tilde{g}| = g_F$. The resulting second pair of magnetic components has the same general characteristics as the first, but with its own optimum $\mathscr{E}_{RF}$ and fine structure, in addition to the different g-factor. Because two independent mechanisms satisfy selection rules (i), there can be interference effects between the two corresponding sets of matrix elements.

The g_P pair and the g_F pair will, in general, have different intensities. The variation of η with (m_P, m_F) within each component makes it very difficult to make a definitive statement regarding the relative intensities. However, it is expected that the intensities will be closely proportional to the number of contributing states, i.e., to the number n of (m_P, m_F) combinations contributing to each component. Here $n = 2$ for g_P and $n = 3$ for g_F. Thus, the g_F pair should be stronger by a factor of 1.5. For each hyperfine system studied, the values of $|\tilde{g}|$ and n are given in Table 4 for the various magnetic pairs possible.

For the purpose of extracting information about the molecule, the hyperfine anticrossings have several disadvantages. First, even for the very small values of $B \gtrsim 2$ mT needed to establish the high field representation for E_α and E_β as shown in Sect. 2A, the spectrum is separated into its magnetic components with the resulting division in intensity. Second, the shape of these components depends on $\mathscr{E}_{RF}$ because the individual lines have different η_{HYP}. As a result, the type of lineshape analysis used to unravel the hyperfine structure in the conventional spectrum (9) cannot be applied here to obtain the hyperfine constants in Δ_{HYP}, except in special cases. Finally, each magnetic component has an rf dependent shift due to Δ_{HYP}. Consequently, the kind of precision studies of E_{ROT} and E_{ST} which are done with the Stark anticrossings cannot be carried out here.

In spite of these difficulties, the hyperfine anticrossings can yield a lot of valuable information. First, by determining the values of $|\tilde{g}|$ for the magnetic components which appear for each system, the selection rules predicted theoretically can be checked experimentally. Second, if $|\eta|$ is large enough that its contribution to [10] can be measured, then accurate values can be obtained for the coupling constant involved in η. If spectra can only be observed where [11] holds, then measurement of the $\mathscr{E}_{RF}$ needed to maximize the component intensity can, in favorable cases, yield an estimate of this coupling constant. Third, for some particular anticrossing, the fine structure of the magnetic components can be analysed in a simple way and Δ_{HYP} measured. For example, this would be the case if

TABLE 5. The Hamiltonian matrix with $m_T = 0$ for the Stark-hyperfine anticrossing problem $(J,K = \pm 2 \leftrightarrow \mp 1, m_J = \pm 1 \leftrightarrow \pm 1)$ hybrid with $(J,K = \pm 2 \leftrightarrow \pm 1, m_J = \pm 1 \leftrightarrow \mp 1)$[a]

K,m_J,m_P,m_F	$-1,+1,-\frac{1}{2},-\frac{1}{2}$	$+2,+1,-\frac{1}{2},-\frac{1}{2}$	$+1,-1,+\frac{1}{2},+\frac{1}{2}$	$-2,-1,+\frac{1}{2},+\frac{1}{2}$
$-1,+1,-\frac{1}{2},-\frac{1}{2}$	$E_{\beta 1}$	η_{ST}	$D_2^{PF}(-1)^*$	$D_1^{PF}(-2)$
$+2,+1,-\frac{1}{2},-\frac{1}{2}$	η_{ST}^*	$E_{\alpha 1}$	$D_1^{PF}(+1)$	0
$+1,-1,+\frac{1}{2},+\frac{1}{2}$	$D_2^{PF}(-1)$	$D_1^{PF}(+1)^*$	$E_{\beta 2}$	η_{ST}
$-2,-1,+\frac{1}{2},+\frac{1}{2}$	$D_1^{PF}(-2)^*$	0	η_{ST}^*	$E_{\alpha 2}$

[a] $D|_{\Delta K}{}^{PF}(K_L)$ is the matrix element of $H_{II}{}^{PF}$, where K_L is the algebraically lower of the two K-values. Explicit expressions are given in the Appendix.

the components consisted of single lines. Fourth, it is not difficult to measure $|2g_{eff}|$ to sufficient accuracy that the terms in $(g_{||} - g_{\perp})$ and/or $g_{\perp}$ are significant in [19]. Since the signs of g_P and g_F are known, the signs of the molecular g-factors can be obtained.

In spite of the complexity of the hyperfine anticrossings, their most important application is perhaps still the determination of $(A_0 - B_0)$. In the approximation used for [16], the crossing field for the hyperfine system $(1,\pm 1,\pm 1) \leftrightarrow (1,0,0)$ in a prolate rotor is given by

$$[21] \quad \mathscr{E}_C = |2h(A_0 - B_0)/\mu|$$

This equation applies to the system $(1,0,\pm 1) \leftrightarrow (1,\pm 1,\mp 1)$ in an oblate rotor if $(A_0 - B_0)$ is replaced by $(B_0 - C_0)$. For both prolate and oblate tops, this is the lowest crossing field possible and, in many cases, is the only one accessible.

Consider a typical experiment in which this one crossing field is measured for a prolate top with $(A_0 - B_0) = 5$ GHz and $\mu = 1$ D, so that $\mathscr{E}_C = 20$ kV/cm. For this anticrossing,

$$[22] \quad \Delta_{ROT} = (A_0 - B_0) - 2D_{JK} - D_K$$

In the final analysis for Δ_{ROT}, assume that corrections are not made for the shifts due to Δ_{HYP} nor for the (J,K) dependence of μ. Furthermore, if $B = 0$, corrections are also omitted for the breakdown of the high-field representation for E_α and E_β, and the failure of the two-level assumption. For a molecule without any quadrupolar terms in H_{HYP}, the neglect of these various corrections will at most degrade the accuracy obtained for Δ_{ROT} from 0.002% by a factor $\lesssim 3$. Even the neglect of D_K in [22] will typically not reduce the accuracy in $(A_0 - B_0)$ below 0.01% or 500 kHz. Thus, although the hyperfine anticrossings cannot be used for some of the most accurate applications of the Stark systems, the values obtained for $(A_0 - B_0)$ are accurate enough for a wide variety of molecular studies.

Because the Stark-hyperfine hybrid systems mentioned in Sect. 2C have some unusual characteristics, and are very useful in the highest precision measurements, the form of the resulting normal spectrum will be considered in detail. These systems involve eight levels in $A \equiv (J,K_\alpha = \pm 2, m_J{}^\alpha = \pm 1)$ and eight levels in $B \equiv (J,K_\beta = \mp 1, m_J{}^\beta = \pm 1)$. Although $(A \leftrightarrow B)$ appears at first glance to be a standard $(\Delta J = 0)$ Stark anticrossing with $K = \pm 2 \leftrightarrow \mp 1$ and $m_J = \pm 1 \leftrightarrow \pm 1$, this is not the case. The 16×16 Hamiltonian matrix factors into three 4×4 blocks with $m_T = -1,0,+1$ and two 2×2 blocks with $m_T = -2,+2$.

The form of the 4×4 block with $m_T = 0$ is shown in Table 5. For $B \gtrsim 2$ mT, the nuclear Zeeman contributions to the diagonal elements make $|E_{\beta 1} - E_{\beta 2}|$ large compared to $|D_2{}^{PF}(-1)|$, so that the system breaks down into two parts, each of which can be treated with the two-level analysis: a Stark anticrossing $(K = \pm 2 \leftrightarrow \mp 1, m_J = \pm 1 \leftrightarrow \pm 1)$ with $|\alpha 1\rangle \leftrightarrow |\beta 1\rangle$ and $|\alpha 2\rangle \leftrightarrow |\beta 2\rangle$ corresponding to upper and lower signs, respectively; and a hyperfine anticrossing $(K = \pm 2 \leftrightarrow \pm 1, m_J = \pm 1 \leftrightarrow \mp 1)$ with $|\alpha 1\rangle \leftrightarrow |\beta 2\rangle$ and $|\alpha 2\rangle \leftrightarrow |\beta 1\rangle$ corresponding to upper and lower signs, respectively. A schematic energy level diagram is shown in Fig. 2. In the hyperfine case, the mixing arises from $\frac{1}{2}(d_{yz}{}^{PF} + d_{zy}{}^{PF})$ as can be seen from Table 3, and η is represented by $D_1{}^{PF}(K)$. For 200 mT $\gtrsim B \gtrsim$ 20 mT, the normal spectrum will consist of four lines, the two Stark lines forming an unresolved doublet at the $(B = 0)$ position and the two hyperfine lines forming a well-resolved magnetic pair with g-factors given in [19].

For $(m_T \neq 0)$, the system is pure Stark in nature and there are no hyperfine anticrossings. The part of the 16×16 matrix with $(m_T \neq 0)$ is identical in form to the corresponding section of the matrix described in Sect. 2C for a Stark system. For example, the 4×4 block with $m_T = +1$ is the same as that shown in Table 2 for the Stark problem except that now $m_J = +1$. This occurs because $\frac{1}{2}(d_{yz}{}^{PF} + d_{zy}{}^{PF})$ cannot introduce any hyperfine mixing. Its selection rule $\Delta m_J = \pm 2$ can be met just as for $m_T = 0$, but it is not possible in this case to satisfy the selection rule $\Delta[m_P + m_F] = \mp 2$ implied by the requirement $\Delta m_T = 0$. Similarly, the 4×4 block with $m_T = -1$ has the structure shown in

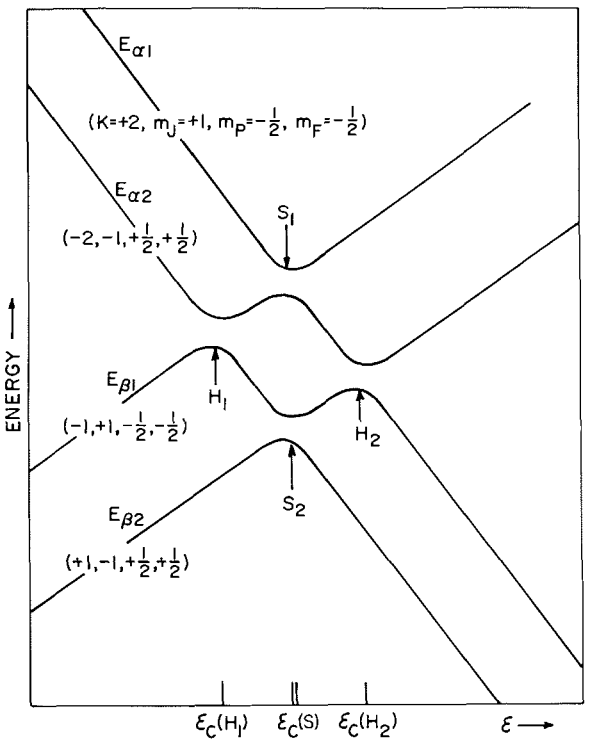

FIG. 2. Schematic plot against $\mathscr{E}$ of the energies of the four interacting levels with ($m_T = 0$) in a hybrid Stark-hyperfine anticrossing. The magnetic field B is large enough that $E_{\alpha 2}$ and $E_{\beta 1}$ are linear with $\mathscr{E}$ in the regions separating the hyperfine anticrossings, H_1 and H_2, from the Stark anticrossings, S_1 and S_2, so that the four can be treated as separate two-level problems. The four minimum separations ν_m have been exaggerated for clarity. $\mathscr{E}_C(S_1)$ is slightly lower than $\mathscr{E}_C(S_2)$. Such a plot would apply for any $J \geq 2$. For ($J = 3$), $[\mathscr{E}_C(H_1) - \mathscr{E}_C(H_2)]$ was used to determine the absolute sign of the rotational g-factors.

Table 2, but with $m_J = -1$. The two 2×2 blocks with $m_T = \pm 2$ are clearly simple two-level Stark anticrossings.

The six anticrossings for $m_T = \pm 1$ and ± 2 combine with the two Stark anticrossings for $m_T = 0$ to form a standard Stark system with all the general characteristics of the pure Stark spectra. The only difference is the presence of the hyperfine magnetic pair. The intensity of each of the hyperfine satellites is 1/8 that of the central Stark line. The mean Stark frequency is at the ($\Delta_Z + \Delta_{HYP} = 0$) position (see Sect. 2*C*), while the mean hyperfine frequency is shifted from the ($\Delta_Z + \Delta_{HYP} = 0$) position by Δ_{HYP}. However, because each magnetic component is a single line, interpretation of this shift does not involve $\mathscr{E}_{RF}$ and so does not face the difficulties mentioned above.

To establish that the two-level assumption is justified for the hyperfine and hybrid anticrossing systems studied, each case must be analysed just as was done for the Stark systems in Sect. 2*C*. The conclusions are similar. The two-level assumption is valid for $B \gtrsim 2$ mT, but for smaller values of B the validity depends on the details. The errors that can be introduced in OPF_3 by using $B < 2$ mT do not significantly affect any of the applications made here. For the hybrid case, where the present requirements are much more stringent, the effect of using very small values of B has been checked experimentally (see Sect. 4).

3. Experimental Considerations: the C-field

The basic mber apparatus used in the current work has been described elsewhere (21). The seeded beam techniques used to obtain the low temperature ($\sim$6 K) required to concentrate the population in the low rotational states have been outlined in earlier reports (1, 9). Here the discussion will be confined to the characteristics and operation of the C-field. These are of particular importance in the anticrossing experiments because they have a direct bearing on the feasibility of observing the spectrum and on the accuracy of measuring the large Stark shifts produced.

The voltage applied to the C-field was taken from two sources, a Fluke #335A and a Fluke #332A, both of which were calibrated to 5 ppm. For measurements below 1100 V, the 332A was used to supply the voltage and the 335A was used as a differential voltmeter to monitor the relative stability of the 332A. For measurements between 1100 and 2100 V/cm, the two supplies were connected in series.

The C-field itself was formed (21) from two optically flat quartz surfaces that were coated first with aluminum and then with gold. This surface is stable for $\mathscr{E} \lesssim 3$ kV/cm, but deteriorates irreversibly at higher fields, producing field inhomogeneities that are unacceptable. In order that the same transition region can be used to study ($\Delta m_T = 0$) spectra for the anticrossings and ($\Delta m_T = \pm 1$) spectra for calibration purposes, the coating procedure for one surface must leave a slit of low conductivity parallel to the beam line. Unfortunately, the slit increased the field inhomogeneities. To overcome this, the quartz plates were coated so as to provide two individual shorter transition regions. The σ section was in the parallel plate configuration which can yield only ($\Delta m_T = 0$) spectra, but gives the more uniform field. The $\pi\sigma$ section contained the slit. The σ region was used for the anticrossings and both regions were used to calibrate (μ_r/d).

This calibration procedure involved the three different frequency measurements. The discussion in Sect. 2*C* following [18] is pertinent at this point.

First, the ($\Delta m_J = 0$) *l*-doubling spectrum (22) of OCS in its first excited bending vibrational state (01^10) was taken on the σ section to measure the ratio of the corresponding moment $\mu_{OCS}{}^E$ to *d*. Then, the ($J_K = 3_{\pm 2}, m_J = \mp 1 \rightarrow 0$) multiplet was selected for OPF_3 as the reference. Both this spectrum and the same OCS spectrum were taken on the $\pi\sigma$ section to give the ratio $\mu_r/\mu_{OCS}{}^E$. The product of the two ratios then gives (μ_r/d) in the form specified in Sect. 2*C*. (μ_r/d) = 2.936318(59) D/cm. A check with the ($J_K = 2_{\pm 1}, m_J = \mp 1 \rightarrow 0$) multiplet as reference gave this same result, but with an error twice as large. The value of *d* itself was 0.636331(23) cm. These calibration numbers, of course, change each time the C-field is disturbed. In order to eliminate the effects of the small contact potentials that arise in mber spectroscopy, all calibration measurements were taken with both polarities and the results averaged. Of course, a similar procedure was followed in the anticrossing measurements themselves.

One of the critical properties of the C-field is its homogeneity. This is illustrated by the typical *normal* spectrum shown in Fig. 3. The optimum $\mathscr{E}_{RF}$ was used. This spectrum is very sensitive to variations in

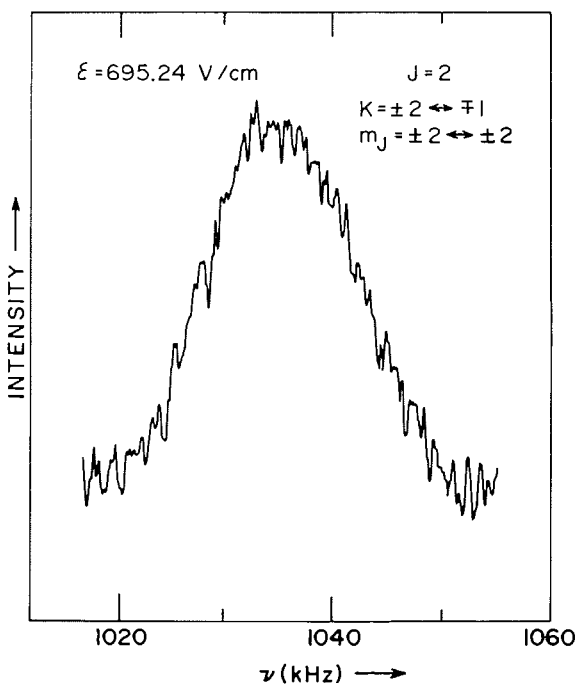

FIG. 3. *Normal* spectrum for a typical Stark anticrossing taken for $\mathscr{E} < \mathscr{E}_C$ in a single sweep with a time constant of 2 s. The full width at half-height $\Delta\nu$ of 18 kHz is determined primarily by the field inhomogeneities. The Stark shift $|\Delta_{ST}| = 652$ MHz, so that the fractional inhomogeneity is better than 3×10^{-5}.

$\mathscr{E}$: s_C = 938.6 kHz/(V/cm). The observed full width $\Delta\nu$ at half-maximum was 18 kHz, whereas the linewidth due to time-of-flight for an isolated line was 7.0 kHz, as calculated (17, 18) from the length, L = 6.2 cm, of the transition region and the velocity, v = 550 m/s, measured (9). Part of the extra width may be due to Δ_{HYP}, which produces a splitting $\lesssim 10$ kHz, where the uncertainty results primarily from the large error in ($c_{\|}{}^P - c_{\perp}{}^P$). However, there is a great deal of evidence that the lineshape is determined primarily by field inhomogeneities. If the entire $\Delta\nu$ in Fig. 3 is assigned to variations in $\mathscr{E}$, then since the magnitude of the Stark shift $|\Delta_{ST}| = 652$ MHz for this anticrossing, the inhomogeneity $\equiv |\Delta\nu/\Delta_{ST}| = 2.8 \times 10^{-5}$. This is of the same order as the accuracy to which the separation *d* of the C-field plates can be adjusted to be constant by simple interferometric methods.

Although the field inhomogeneities dominate the lineshape, these effects did not introduce any serious asymmetries. As a result, they did not appreciably degrade the accuracy of the final results from the Stark crossings. For the *absolute* measurements of $\Delta_{ROT}{}^A$ required to determine *a* in [18], the error in the typical frequency measurement must be $\lesssim (\Delta\nu/4)$ in order that this error be negligible compared to the already existing limit of $1\text{–}2 \times 10^{-5}$ due to the long-term stability of the voltage source. The resulting requirement on the symmetry is easily met. For *relative* measurements of $\Delta_{ROT}{}^A$ required to determine *b* in [18], the limit from the voltage source is the short term stability of 2×10^{-6}. At this level, the lineshape distortions can introduce significant errors in individual frequencies. However, only frequency *differences* need to be found. Because both spectra involved here always have the same s_C, the asymmetry errors cancel to the required accuracy.

In studies of the hyperfine anticrossings, the inhomogeneities have a much larger effect. Among other things, the large $\Delta\nu$ eliminates the possibility of resolving the fine structure due to Δ_{HYP}.

In general, the uniformity of $\mathscr{E}$ can be an important factor in determining the feasibility of measuring ($A_0 - B_0$). In [21], the lowest crossing field available for any particular symmetric top under study is given. Let us consider a group of molecules with the same μ but different ($A_0 - B_0$) and ask which aspect(s) of the anticrossing technique limits the largest ($A_0 - B_0$) that can be measured. If the population and focussing properties of state $|\beta\rangle$ provide enough molecules to produce a strong spectrum in an ideal C-field, then this upper limit to ($A_0 - B_0$) is set by the line width $\Delta\nu$ of the real C-field due to its inhomogeneity. As ($A_0 - B_0$) increases, $|\Delta_{ST}|$ will go up and $\Delta\nu$ will get larger at

least as quickly. The lowest frequency at which the anticrossing spectrum can be studied is $\gtrsim 2\Delta\nu$. Thus as $(A_0 - B_0)$ increases, this minimum frequency will go up. The optimum $\mathscr{E}_{RF}$ required will increase both *directly* as it would in a conventional mber experiment because the ratio of the inhomogeneous and homogeneous widths has gone up, and *indirectly* as indicated by [12] because v has gone up. Eventually $(A_0 - B_0)$ will become so large that the value of $\mathscr{E}_{RF}$ required cannot be generated. For the present C-field, the homogeneity requirements can be met for $\mathscr{E} \lesssim 3$ kV/cm, so that $(A_0 - B_0) \lesssim 750$ MHz for $\mu = 1$ D. However, with techniques currently available for the construction of C-fields, these requirements can be met for fields as large as 20 kV/cm, so that $(A_0 - B_0) \lesssim 5$ GHz for $\mu = 1$ D.

4. Results

A. The Stark Crossing Fields

A series of Stark anticrossings of the type $(J,K_\alpha = \pm 2,m_J) \leftrightarrow (J,K_\beta = \mp 1,m_J)$ were studied to obtain $(A_0 - B_0)$ and μ_J. For each anticrossing, the *absolute* crossing voltage V_C and the *apparent* rotational energy difference $\Delta_{ROT}{}^A$ defined in [18] are given in Table 6 along with the number N_m of independent measurements made. For each case, at least one of the measurements was made by the *above/below* method described in Sect. 3.

All the data were taken in the earth's magnetic field. Because B was so small, the measurement of V_C obtained for each case with $m_J = \pm 1$ represents the hybrid Stark-hyperfine value. However, by applying an external magnetic field $\gtrsim 20$ mT, it was shown that there is no significant difference from the V_C for the pure Stark system (see Sect. 2*D*).

The internal consistency of the data is very good. For many of the crossings, runs were taken a week (or several weeks) apart, but the standard deviations fall generally between 2 and 6 kHz. For $J = 2$, the values of $\Delta_{ROT}{}^A$ for the two different $|m_J|$ agree to within 2 kHz. For $J = 3$, the values of $\Delta_{ROT}{}^A$ for the three different $|m_J|$ agree to 4 kHz. For comparison, 6.5 kHz is 0.001%. This indicates that the long term stability and reproducibility of the voltage supplies is a factor of 2–4 better than the upper limit of 2×10^{-5} listed in the manufacturer's specifications.

The *relative* measurements made to determine directly differences in $\Delta_{ROT}{}^A$ are summarized in Table 7. Here $(J_1 m_{J,1})$ and $(J_2 m_{J,2})$ label the two systems in Table 6 that are being compared. The errors in $[\Delta_{ROT}{}^A(J_2) - \Delta_{ROT}{}^A(J_1)]$ are dominated by the short term stability of the voltage source for the first three cases. For the case involving $J = 8$, the error is dominated by the uncertainty in finding the centre of the very weak line for this rather high J. A spectrum for $(J_2 = 8)$ is shown in Fig. 4 along with one taken in the same field for $(J_1 = 3)$. Table 7 also lists the values obtained for b using [18].

A least-squares fit was made to the combined data on $\Delta_{ROT}{}^A$ in Tables 6 and 7 to obtain a and b. The absolute values of $\Delta_{ROT}{}^A$ in Table 6 were taken to be internally consistent to 0.001% based on the performance of the voltage sources and so were assigned errors of 6.5 kHz for weighting purposes. It was found that $a = 217\,499.60(72)$ kHz and $b = 0.904(12)$ kHz; the errors shown are those given by the least-squares fit. For each J, the results given in Table 8 were obtained with [18] from the average value of $\Delta_{ROT}{}^A$ for that J in Table 6. In the calculation, the known values of D_{JK} and D_K given in Table 1 were used. The reference transition enters the calculation through ε in [18*e*]. Since $J_r = 3$ and $K_r = \pm 2$, as indicated in Sect. 3, $\varepsilon = 12(\mu_J/\mu_0) + (\mu_K/\mu_0)$. In calculating $(A_0 - B_0)$, it was assumed that $|\mu_K| \sim |\mu_J|$ and that the term in μ_K could consequently be dropped. In Table 8, the values of $(A_0 - B_0)$ have a spread of less than 7×10^{-6}, as compared with the manufacturer's specification of 2×10^{-5} for the long term stability of the supplies.

The final values of $(A_0 - B_0)$ and μ_J, as calculated from the least-squares results for a and b, are given

TABLE 6. Absolute crossing voltages and apparent rotational energy differences for the Stark anticrossings $(K = \pm 2 \leftrightarrow \mp 1)$

J	m_J	N_m[a]	V_C (V)[b,c]	$\Delta_{ROT}{}^A$ (kHz)[b]
2	± 1[d]	6	870.4613(53)	652 485.8(4.1)
2	± 2	2	441.9291(41)	652 484.3(6.1)
3	± 1[d]	3	1736.3708(61)	652 467.2(2.3)
3	± 2	2	880.9629(5)	652 467.0(0.4)
3	± 3	1	588.9384[e]	652 463.0[e]
4	± 4	2	735.9814(19)	652 445.0(1.7)
5	± 5	3	883.0236(12)	652 416.5(0.9)
6	± 6	2	1030.0595(45)	652 383.8(2.9)
8	± 6	2	1765.0208(69)	652 301.7(2.6)

[a] $N_m \equiv$ total number of measurements.
[b] The error shown represents only the standard deviation for the N_m different measurements. The absolute errors are ~0.002%. In $\Delta_{ROT}{}^A$, this is ~13 kHz.
[c] To obtain $\mathscr{E}_C$, V_C must be divided by $d = 0.626331(23)$ cm.
[d] These are hybrid Stark-hyperfine systems, but the results are given for the pure Stark component (see Sect. 2*D*).
[e] No standard deviation is given because $N_m = 1$.

TABLE 7. Relative measurements for Stark crossings $(K = \pm 2 \leftrightarrow \mp 1)$ to determine μ_J[a]

J_1	$m_{J,1}$	J_2	$m_{J,2}$	$\Delta_{ROT}{}^A(J_2) - \Delta_{ROT}{}^A(J_1)$ (kHz)	b (kHz)
2	± 1	3	± 2	−15.7(1.5)	0.874(83)
3	± 2	5	± 5	−49.5(1.5)	0.917(28)
2	± 1	5	± 5	−63.9(1.5)	0.887(21)
3	± 1	8	± 6	−163.3(3.0)	0.907(17)

[a] See Sect. 2*C* and [18] in particular for definitions of the symbols.

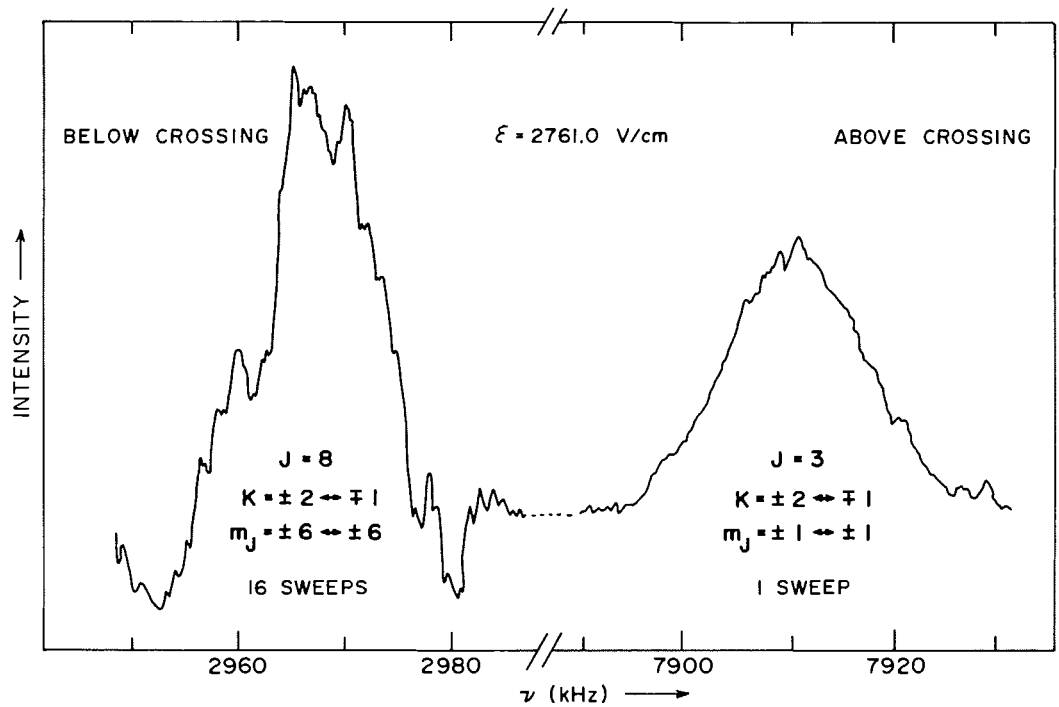

FIG. 4. Spectra for two different Stark anticrossings in the same electric field. The $J = 8$ curve is *normal* and the $J = 3$ curve is *inverted*. There is a break in the frequency axis; each section has its own frequency scale and intensity scale. The runs were taken in the earth's magnetic field. Relative measurements such as this were used to determine μ_J.

in Table 1. The error in $(A_0 - B_0)$ is, of course, limited to 2×10^{-5} by the long term characteristics of the voltage sources. Two other determinations of $(A_0 - B_0)$ are given in Table 1. The agreement is very satisfying, particularly with the distortion moment spectroscopy result.

B. The Stark Minimum Separations

For the Stark anticrossings $(J,K_\alpha = \pm 2,m_J = J) \leftrightarrow (J,K_\beta = \mp 1,m_J = J)$, the minimum separation is given by (see [13]):

$$[23] \quad \nu_m = \mu_D \mathcal{E}_C J[(J-1)(J+2)]^{1/2}$$

For $J \geq 4$, ν_m is large enough compared to $\Delta\nu$ that the transition frequency could be measured accurately right through the crossing. This was done for $J = 4$ and $J = 6$. A spectrum taken for $J = 4$ just below $\mathcal{E}_C$ is shown in Fig. 5. For each J, the data were analysed with [10] to obtain V_C and $|\eta| = \nu_m/2$. The quality of the fit was good in each case; the fit for $J = 6$ is illustrated in Fig. 6. For $J = 4$, $\nu_m = 57.64(66)$ kHz and $\mu_D = 5.835(67) \times 10^{-6}$ D. For $J = 6$, $\nu_m = 181.14(65)$ kHz and $\mu_D = 5.858(20) \times 10^{-6}$ D. The weighted average is given in Table 1. The agreement between the two values for μ_D shows that the J-dependence given in [23] is correct and confirms that the mixing is due to the distortion dipole mechanism. Measurements on a single anticrossing cannot provide this information.

On the basis of qualitative arguments (23), it is expected that the rotational contribution Θ_{ROT} to μ_D in [14] will be dominant in heavy molecules such as OPF_3 with large μ_0 and small $(A_0 - B_0)$. The current measurement of $|\mu_D|$ makes it possible to test this argument for the first time. From the harmonic force field, it was found (10) that $\tau_{yyyz}' \equiv (\hbar^4\tau_{yyyz}/h) = 1.28$ kHz.[10] From this result and the parameters given in Table 1, $|\Theta_{ROT}| = 5.50 \times 10^{-6}$ D, which differs by only 6% from $|\mu_D|$. If one makes the reasonable assumption that μ_D and Θ_{ROT} have the same sign, then indeed $|\Theta_{ROT}| \gg |\Theta_y^{yy}|$, as expected. However, some of the $\Theta_\alpha^{\beta\gamma}$ are of the same order of magnitude as Θ_{ROT}. This can be deduced from the fact that $|\mu_J| \sim |\mu_D|$ (see Table 1) and the definition of μ_J in [5*b*]. Further insight into this question can be obtained by measuring μ_D and μ_J in $^{18}OPF_3$.

[10] In relating the τ' used here to the τ' used in other works, one must first take into account the change in coordinate system pointed out in footnote 7. If this is done, then τ_{yyyz}'(here) $= \tau_{xxxz}'(10) = \tau_{xxxz}'(11) = 4\tau_{xxxz}'(12)$. Although the force-field value was used in the current work, the relationship to the definition of τ_{xxxz}' used in ref. 10 was established only after a correction to the original paper was made in [8] of ref. 10: $\tau_{xxxz}' = 4q_3$ rather than $2q_3$. The assistance of Dr. J. G. Smith on this point was very helpful.

TABLE 8. Final determination of $(A_0 - B_0)$ from the Stark crossings $(K = \pm 2 \leftrightarrow \mp 1)$

J	$(A_0 - B_0)$ [a] (kHz)	$(A_0 - B_0)(\mu_J/\mu_0)J(J+1)$ [b] (kHz)
2	217 499.60	−2.36(7)
3	217 498.55	−4.72(14)
4	217 498.85	−7.86(24)
5	217 498.45	−11.79(36)
6	217 498.35	−16.51(50)
8	217 498.15	−28.30(86)

[a]The estimated error in each entry for relative purposes is 0.001% or 2 kHz. The absolute error is 0.002% or 4 kHz.
[b]This is the contribution of μ_J to $(\Delta_{ROT}{}^{\wedge}/3)$ as calculated with $b = 0.904(12)$ kHz (see [18]).

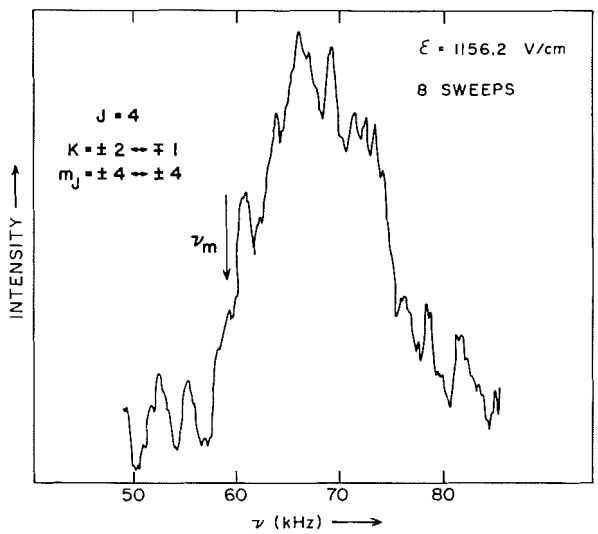

FIG. 5. Spectrum for a Stark anticrossing taken with $\mathscr{E}$ just below $\mathscr{E}_C$. The value of the minimum separation ν_m was determined to be 57.64(66) kHz. Because the line is so close to the crossing, $|\partial\nu/\partial\mathscr{E}|$ is small compared to $|s_C|$ and the line width $\Delta\nu$ is narrower than in spectra taken far from $\mathscr{E}_C$.

C. *The Hyperfine Anticrossing: General Studies and Selection Rules*

All the hyperfine anticrossings listed in Table 4 were studied in detail with $B \lesssim 10$ μT. The hyperfine spectra observed were typically weaker than the stronger of the Stark spectra by a factor of 10 or more. The low value of B was selected in these initial experiments to avoid the intensity division produced by the very fast magnetic splitting. In each case, the crossing field $\mathscr{E}_C$ was measured. To improve the accuracy, each measurement with one exception was made *relative* to a convenient Stark $\mathscr{E}_C$. The exception was the $(J = 1)$ hyperfine avoided crossing for which no nearby Stark reference was available. Unfortunately, because of the difficulties pointed out in Sect. 2*D*, no information on Δ_{HYP} could be extracted. Furthermore, although values of $(A_0 - B_0)$ were obtained in agreement with those determined from the Stark anticrossings, the accuracy was not competitive. Serious attempts were made to follow the transitions close enough to $\mathscr{E}_C$ that the contribution from η in [10] would become significant, but in each case $|\eta|$ was too small relative to Δν.

All these hyperfine anticrossings were then studied with $B \geq 20$ mT. Because the individual components were now even weaker, no attempt was made to determine Δ_{HYP} or to make precision measurements of $(A_0 - B_0)$. Effort was concentrated on checking the selection rules derived in Sect. 2*D* and summarized in Tables 3 and 4. All of the magnetic components listed in Table 4 were observed except the two marked with asterisks. The relative intensities obtained are given in Table 4. Because of the difficulty in optimizing $\mathscr{E}_{RF}$ on such weak lines, these measurements must be regarded as estimates of the true relative strengths with an uncertainty the order of a factor of two.

For the four cases in Table 4 in which more than one magnetic pair were observed in a single anticrossing system, the relative intensities were proportional (within the rather large error) to the ratio of the corresponding n's as predicted in Sect. 2*D*. For $(J = 2, K = \pm 2 \leftrightarrow 0, m_J = \pm 2 \leftrightarrow 0)$, the agreement is illustrated in Fig. 7. All four magnetic components have about the same intensity with individually optimized $\mathscr{E}_{RF}$ and n is the same for both magnetic pairs. For $(J = 1, K = \pm 1 \leftrightarrow 0, m_J = \pm 1 \leftrightarrow 0)$, the g_F and g_P pairs were observed to be of equal strength, and the n-ratio for g_F to g_P is 3:2. For both of the hybrid Stark-hyperfine cases, the hyperfine satellites were ~1/8 the intensity of the pure Stark component, as expected (see Sect. 2*D*).

The two "missing" magnetic components, both with $|\tilde{g}| = g_P$, were expected to be very weak. The relative intensity predicted from the corresponding observed g_F pair using the n-ratio is given in Table 4. Even with prior knowledge[11] of the optimum $\mathscr{E}_{RF}$, these require ~1 h of averaging to see the line. For $(J = 1, K = \pm 1 \leftrightarrow 0, m_J = \pm 1 \leftrightarrow 0)$ where the g_P pair was observed and is of about the same strength as the missing cases, the $\mathscr{E}_{RF}$ used was first set at the value for its g_F partners and this proved to be close to the optimum. When the same procedure was used for $(J = 2, K = \pm 1 \leftrightarrow 0, m_J = \pm 1 \leftrightarrow 0)$, it failed. Subsequent calculations showed that the $\mathscr{E}_{RF}$ used was about a factor of four too low.

For each hyperfine anticrossing system studied, a search was made for all conceivable magnetic components other than those predicted. None were

[11]In conventional mber work, a very high $\mathscr{E}_{RF}$ can often be used to observe weak lines for the first time and then reduced later. In the anticrossing spectra, a variety of effects obscure the lines if $\mathscr{E}_{RF}$ is much larger than the optimum value.

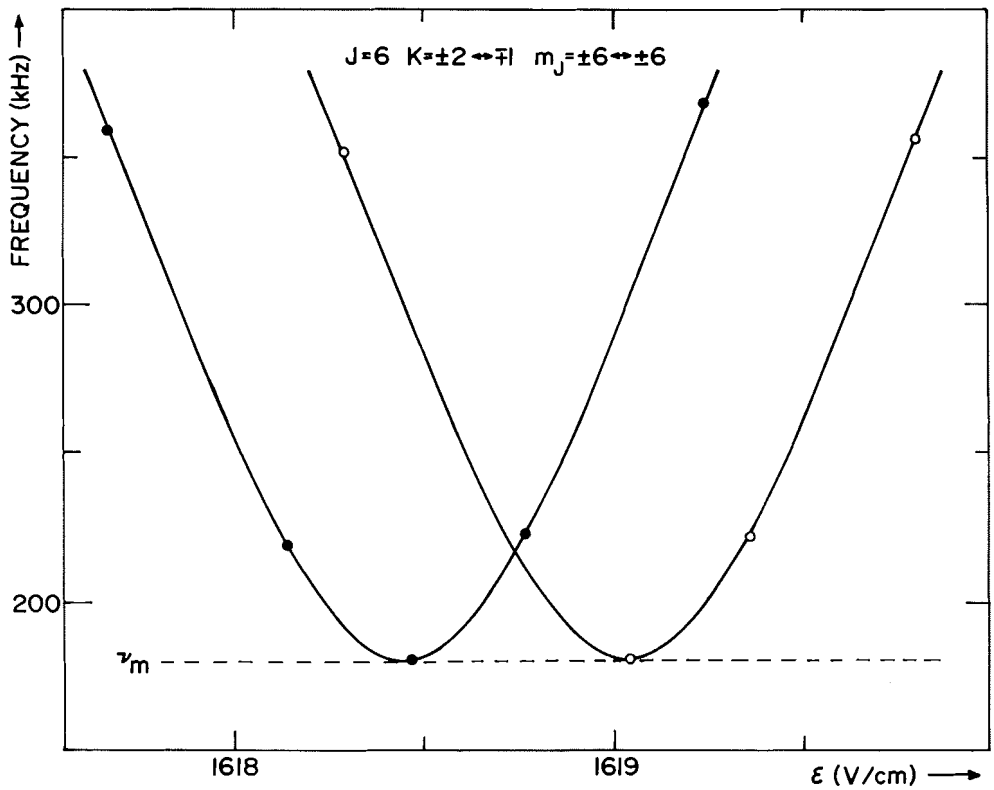

FIG. 6. The determination of ν_m for the Stark crossing ($J = 6$, $K = \pm 2 \leftrightarrow \mp 1, m_J = \pm 6 \leftrightarrow \pm 6$). The experimental data were taken separately for each polarity of the C-field, the dots for positive polarity and the open circles for negative polarity. The solid curves are the least-squares fits, yielding $\nu_m = 181.04(68)$ and 181.25(83) kHz, respectively. The mean value of $\mathscr{E}_C$ is 1618.743 V/cm.

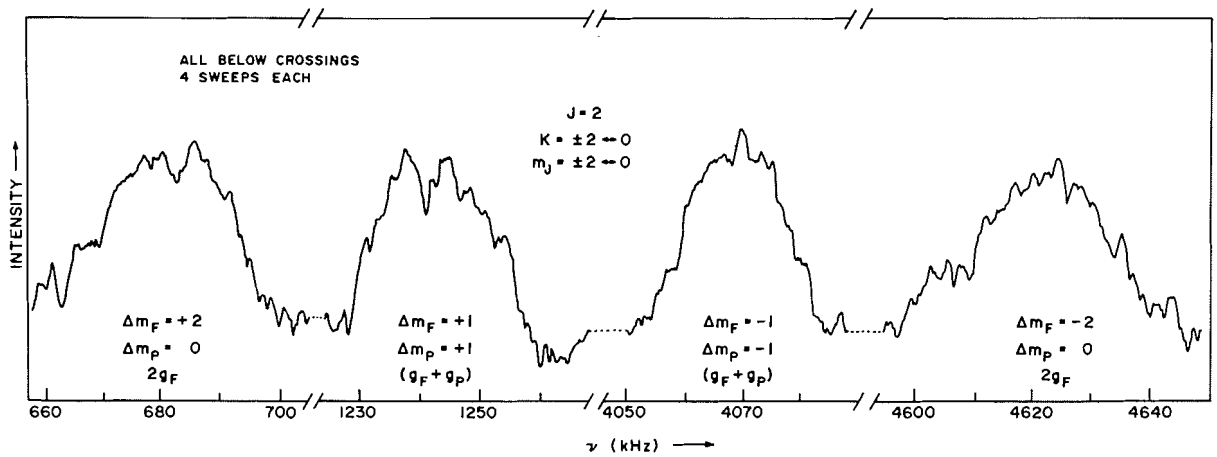

FIG. 7. *Normal* spectrum for hyperfine anticrossing taken with $\mathscr{E} = 1362.4$ V/cm and $B = 24.4$ mT. Each magnetic component has its own frequency scale, but the same intensity scale applies to the different sections. There are two pairs of magnetic components, one with $|\tilde{g}| = (g_F + g_P)$ and one with $|\tilde{g}| = 2g_F$. The ratio of the two splittings has been used to determine the sign of the rotational g-factors.

found. In view of the intensity problems just mentioned, this result cannot be taken as definitive proof that these other selection rules are forbidden. However, the selection rules derived in Sect. 2*D* are certainly consistent with all the experimental evidence.

If a single hyperfine mechanism provides the mixing, then a measurement of the optimum $\mathscr{E}_{RF}$ can provide a value for the corresponding coupling constant through [12]. This was done for the g_F components of the first two systems listed in Table 4. This gave $\frac{1}{2}(c_{yz}^F + c_{zy}^F) = 4.8$ and 4.3 kHz from the $J = 1$ and 2 data, respectively. Such results can be very unreliable, particularly when Δv is determined by field inhomogeneities. To test the reliability, the same technique was applied to all the Stark systems studied, where the mixing is known from the measurement of μ_D. It was found that the method was reliable to about a factor of two. To be conservative, however, the final value for $\frac{1}{2}(c_{yz}^F + c_{zy}^F)$ of 4.5 kHz should be regarded as an order of magnitude estimate. This is in itself of considerable interest because no constant of this type has been measured before (to our knowledge).

D. The Sign of the Rotational g-factors

The absolute signs of $g_\perp$ and $g_\parallel$ were determined by studying the hyperfine satellites of the hybrid system ($J = 3, K = \pm 2 \leftrightarrow \pm 1, m_J \pm 1 \leftrightarrow \mp 1$). A schematic plot of the energy levels is shown in Fig. 2. In a field of 40.185(18) mT, the splitting between the two magnetic components was 4655.0(2.0) kHz, so that $|g_{eff}| = 7.5985(47)$ nm. From [19], the rotational contribution g_R to $|g_{eff}|$ is $(19g_\perp + 5g_\parallel)/24$. By using the values for the nuclear *g*-factors (24) and shielding (25–27) together with [19], it was found from this experimental value of $|g_{eff}|$ that $g_R = -0.0410(24)$ nm. From earlier work (9) which gave the magnitudes of $g_\perp$ and $g_\parallel$ as well as showing $(g_\perp/g_\parallel) > 0$, it was calculated that $|g_R| = 0.04233(7)$ nm. The two magnitudes are in agreement. The negative sign for g_R shows that $g_\perp$ and $g_\parallel$ are both negative. This conclusion was confirmed by a similar study of the hyperfine system ($J = 2, K = \pm 2 \leftrightarrow 0, m_J = \pm 2 \leftrightarrow 0$) using spectra such as that shown in Fig. 7.

5. Conclusion

The principal purpose of the present work was to develop a new method of measuring A_0 (or C_0) in a symmetric rotor. OPF_3 was selected for this initial study primarily for two reasons: the crossing fields are conveniently low and a precision comparison value was available[5] from distortion moment spectroscopy (11). Because of the agreement for $(A_0 - B_0)$ to within the current accuracy of 0.002% with the microwave value given in Table 1 and because of the internal consistency of the anticrossing data, the method is considered to be now established.

Several other techniques of measuring A_0 (or C_0) with high precision have been developed over the past decade. A brief comparison with three of these has been given in ref. 1: (I) distortion moment microwave spectroscopy; (II) infrared studies of perturbation-allowed vibration–rotation transitions; (III) Raman spectroscopy. A fourth method is based on microwave studies of perturbation-allowed pure rotational transitions in excited vibrational states. A recent example is the determination (28) for NSF_3 of A_v for both the ($v_5 = 1$)and the ($v_6 = 1$) states. This approach can be used for molecules with even very large $(A_0 - B_0)$ and/or relatively small μ. On the other hand, it requires an accidental near-degeneracy which permits the observation of ($\Delta K = \pm 3$) transitions whose frequencies are sensitive to A_v. A very complex spectrum must be analysed and, to obtain A_0 (or C_0) itself, a correction must be made. In spite of these difficulties, this technique is being rapidly developed and has been successfully applied to a number of molecules.

A fifth method involves the study (12) with laser-Stark spectroscopy of the same type of anticrossings as are investigated here with mber. The laser-Stark and beam techniques are similar in many respects, and it is not at all clear which will ultimately be the more powerful. With a fixed frequency laser, the electric field in the laser-Stark method must simultaneously satisfy two conditions. First, it must shift the rotation–vibration transition in question so that the laser line is within the transition's Doppler profile. Second, it must bring the two anticrossing levels to their crossing field. This difficulty will be overcome when suitable tunable lasers become available. The two methods are limited in different ways with regard to the range of values of $(A_0 - B_0)$, μ, and J that can be studied. In the laser Stark experiment of ref. 12, a larger mixing is required, in part because the line width is larger by a factor of ~ 10 and in part because the modulation frequency is higher (10 kHz as compared to 20 Hz). The two sets of anticrossings observed in ref. 12, both Stark, had $|\eta| = 831$ kHz for $J = 13$ and 389 kHz for $J = 10$, as calculated from the current value of μ_D. On the other hand, the mber method is confined to rather lower J values. If adequate mixing is available for $J = 2$ (the lowest J that has a ($\Delta J = 0$) Stark anticrossing), then the laser-Stark experiment can go as high as 12 GHz in $(A_0 - B_0)$ for $\mu = 1$ D. For comparison, the beam experiment should be able to reach 5 GHz with the ($J = 1$) hyperfine anticrossing.

Both of these limits are set by current technical considerations and not by fundamental difficulties. As the two methods develop, they should complement each other rather well.

Avoided-crossing spectroscopy has also been used to study spherical tops using a magnetic-resonance molecular-beam spectrometer (29). In this case, the difference in the Zeeman energies is used to cancel the difference in rotational energies. The systems investigated to date are three level problems which are hyperfine anticrossings if $\mathscr{E} = 0$ and hybrid Stark-hyperfine anticrossings if $\mathscr{E} \neq 0$. These experiments have yielded, for example, the distortion dipole moment and proton spin rotation constants of CH_4.

Now that the anticrossing mber method of measuring $(A_0 - B_0)$ in symmetric tops is established, the technique will be applied to a series of molecules with $(A_0 - B_0)$ or $(B_0 - C_0) \lesssim 5$ GHz and $\mu \sim 1$ D. The method will also be used to investigate internal rotation, developing this aspect of the technique as first applied to CH_3CF_3 (8).

6. Acknowledgements

The authors wish to thank Dr. A. Dymanus for many stimulating discussions. One of us (I.O.) would like to thank both the National Research Council of Canada for a travel grant covering the earlier period when the experimental work was done and the Natural Sciences and Engineering Research Council of Canada for its research support during the later period when a great deal of the analysis was carried out and the manuscript was written. Both authors wish to thank the North Atlantic Treaty Organization Research Grant Programme for its support during this later period.

1. I. OZIER and W. L. MEERTS. Phys. Rev. Lett. **40**, 226 (1978).
2. J. K. G. WATSON. J. Mol. Spectrosc. **40**, 536 (1971).
3. M. R. ALIEV and V. M. MIKHAYLOV. J. Mol. Spectrosc. **49**, 18 (1974).
4. J. K. G. WATSON, M. TAKAMI, and T. OKA. J. Chem. Phys. **70**, 5376 (1979).
5. Y. UEDA and K. SHIMODA. Laser spectroscopy. *In* Proceedings of the Second International Conference, Megève, June 25–27, 1975. Springer-Verlag, New York, NY. 1975.
6. K. LALITA and T. OKA. Phys. Can. **32**, 18 (1976).
7. W. H. FLYGARE and R. C. BENSON. Mol. Phys. **20**, 225 (1971).
8. W. L. MEERTS and I. OZIER. Phys. Rev. Lett. **41**, 1109 (1978).
9. W. L. MEERTS, I. OZIER, and A. DYMANUS. Can. J. Phys. **57**, 1163 (1979).
10. J. G. SMITH. Mol. Phys. **32**, 621 (1976).
11. R. H. KAGANN, I. OZIER, and M. C. L. GERRY. J. Mol. Spectrosc. **71**, 281 (1978).
12. T. AMANO and R. H. SCHWENDEMAN. J. Mol. Spectrosc. **78**, 437 (1979).
13. T. AMANO and R. H. SCHWENDEMAN. J. Chem. Phys. **68**, 530 (1978).
14. S. C. WOFSY, J. S. MUENTER, and W. KLEMPERER. J. Chem. Phys. **53**, 4005 (1970).
15. E. R. COHEN and B. N. TAYLOR. J. Phys. Chem. Ref. Data, **2**, 663 (1973).
16. W. GORDY and R. L. COOK. Microwave molecular spectra. Interscience, New York, NY. 1970.
17. N. F. RAMSEY. Molecular beams. Oxford University Press, London, Engl. 1956.
18. H. C. TORREY. Phys. Rev. **59**, 293 (1941).
19. T. C. ENGLISH and J. C. ZORN. *In* Methods of experimental physics. Vol. 3. *Edited by* D. Williams. Academic Press, New York, NY. 1973.
20. J. P. GORDON. Phys. Rev. **99**, 1253 (1955); S. G. KUKOLICH and S. C. WOFSY. J. Chem. Phys. **52**, 5477 (1970).
21. F. H. DE LEEUW and A. DYMANUS. J. Mol. Spectrosc. **48**, 427 (1973); F. H. DE LEEUW. Ph.D. Thesis. Katholieke Universiteit, Nijmegen, The Netherlands. 1971.
22. J. M. L. J. REINARTZ and A. DYMANUS. Chem. Phys. Lett. **24**, 346 (1974).
23. F. Y. CHU and T. OKA. J. Chem. Phys. **60**, 4612 (1974).
24. G. H. FULLER. J. Phys. Chem. Ref. Data, **5**, 835 (1976).
25. M. R. BAKER, C. H. ANDERSON, and N. F. RAMSEY. Phys. Rev. **133**, A1533 (1964).
26. J. W. EMSLEY, J. FEENEY, and L. H. SUTCLIFFE. High resolution N.M.R. spectroscopy. Pergamon Press, Oxford, Engl. 1966.
27. A. MÜLLER, E. NIECKE, and B. KREBS. Mol. Phys. **14**, 591 (1968).
28. C. E. SMALL and J. G. SMITH. Mol. Phys. **37**, 665 (1979).
29. I. OZIER. Phys. Rev. Lett. **27**, 1329 (1971); W. M. ITANO and I. OZIER. J. Chem. Phys. **72**, 3700 (1980); W. M. ITANO and N. F. RAMSEY. J. Chem. Phys. **72**, 4941 (1980).
30. A. W. ELLENBROEK and A. DYMANUS. Chem. Phys. **35**, 227 (1978); A. W. ELLENBROEK. Ph.D. Thesis. Katholieke Universiteit, Nijmegen, The Netherlands. 1977.
31. E. U. CONDON and G. M. SHORTLEY. Theory of atomic structure. Cambridge University Press, New York, NY. 1964.
32. A. R. EDMONDS. Angular momentum. Princeton University Press, Princeton, NY. 1957.
33. P. B. DAVIES, R. M. NEUMANN, S. C. WOFSY, and W. KLEMPERER. J. Chem. Phys. **55**, 3564 (1971).
34. W. H. FLYGARE. J. Chem. Phys. **41**, 793 (1964).

Appendix: Matrix Elements of the Hyperfine Hamiltonian Off-diagonal in K

The matrix elements of H_{HYP} off-diagonal in K have been calculated in the high-field representation discussed in Sect. 2*A*. Although the basis functions ψ have been discussed elsewhere (14, 30), the specific form adopted here will be summarized briefly so that full use can be made of the matrix elements in other applications.

$$[A1] \quad \psi = \chi_P(I_P m_P)\chi_F{}^{\Gamma,K}(I_F m_F)R(J,K,m_J)$$

Here the first two factors are the phosphorus and fluorine spin functions. If $|K| = 3N$, then χ_F transforms by irreducible representation $\Gamma = A_1$ and $I_F = 3/2$. If $|K| \neq 3N$, $\Gamma = E$ and $I_F = \frac{1}{2}$. In the usual notation for writing the spin functions of the individual fluorine spins with the conventions of Condon and Shortley (31),

[A2] $\chi_F^{A_1}(\frac{3}{2}, \frac{3}{2}) = \alpha\alpha\alpha$

[A3] $\chi_F^{E,K}(\frac{1}{2}, \frac{1}{2}) = (1/\sqrt{3})[\beta\alpha\alpha + \alpha\alpha\beta \times \exp(2\pi Ki/3) + \alpha\beta\alpha \exp(4\pi Ki/3)]$

The functions for the other values of m_F can be obtained by simple ladder operations. The last factor in [A1] is the rotational function. In the conventions defined by Edmonds (32),

[A4] $R(J,K,m_J) = \left[\frac{2J+1}{8\pi^2}\right]^{1/2} \mathscr{D}_{m_J K}^{(J)}$

Except for the case $K = 0$, the basis functions do not have A_1 or A_2 symmetry, but are a mixture. For $K = 0$, ψ is of A_1 or A_2 symmetry (corresponding to J even and J odd, respectively). This behaviour is to be contrasted with that of the zero-field basis set where all the functions are of symmetry A_1 or A_2.

The methods used to calculate the matrix elements are essentially the same as those employed in refs. 14, 30, and 33. The matrix elements diagonal in J, $|K|$, and I_F are given in refs. 14, 32, and 9 in a form consistent with the current work and are not reproduced here. The matrix elements off-diagonal in K and I_F (but diagonal in J) are listed below.

Fluorine Spin–Rotation Interaction

$$[A5]\quad \langle JKm_J I_P m_P I_F m_F|H_{IJ}^{F}|JK'm_J' I_P m_P' I_F' m_F'\rangle = \{\tfrac{1}{2}i(c_{yz}^{F} + c_{zy}^{F})\delta(|K-K'|,1) + \tfrac{1}{2}(c_{xx}^{F} - c_{yy}^{F}) \times \delta(|K-K'|,2)\}\delta(m_P,m_P')\delta(m_J + m_F, m_J' + m_F')(-1)^{\tau_F}(2J+1)\sqrt{30J(J+1)(2J+1)} \times \begin{Bmatrix} 1 & 1 & 2 \\ J & J & J \end{Bmatrix} \begin{pmatrix} J & 2 & J \\ -K & K-K' & K' \end{pmatrix} \begin{pmatrix} J & 1 & J \\ -m_J & m_J - m_J' & m_J' \end{pmatrix} \begin{pmatrix} I_F & 1 & I_F' \\ -m_F & m_F - m_F' & m_F' \end{pmatrix}$$

where

$$\tau_F = J - K + J - m_J + I_F + \tfrac{1}{2} + I_F' - m_F'$$

Phosphorus–Fluorine Spin–Spin Interaction

$$[A6]\quad \langle JKm_J I_P m_P I_F m_F|H_{II}^{PF}|JK'm_J' I_P m_P' I_F' m_F'\rangle = \{\tfrac{1}{2}i(d_{yz}^{PF} + d_{zy}^{PF})\delta(|K-K'|,1) + \tfrac{1}{2}(d_{xx}^{PF} - d_{yy}^{PF}) \times \delta(|K-K'|,2)\}(-1)^{\tau_{PF}}(2J+1)\sqrt{30I_P(I_P+1)(2I_P+1)} \begin{pmatrix} 1 & 1 & 2 \\ m_P - m_P' & m_F - m_F' & m_J' - m_J \end{pmatrix} \times \begin{pmatrix} J & 2 & J \\ -K & K-K' & K' \end{pmatrix} \begin{pmatrix} J & 2 & J \\ -m_J & m_J - m_J' & m_J' \end{pmatrix} \begin{pmatrix} I_P & 1 & I_P \\ -m_P & m_P - m_P' & m_P' \end{pmatrix} \begin{pmatrix} I_F & 1 & I_F' \\ -m_F & m_F - m_F' & m_F' \end{pmatrix}$$

where

$$\tau_{PF} = J - K + J - m_J + I_P - m_P + I_F - m_F + I_F' + \tfrac{1}{2}.$$

Fluorine–Fluorine Spin–Spin Interaction

$$[A7]\quad \langle JKm_J I_P m_P I_F m_F|H_{II}^{FF}|JK'm_J' I_P m_P' I_F' m_F'\rangle = \{\tfrac{1}{2}i(d_{yz}^{FF} + d_{zy}^{FF})\delta(|K-K'|,1) + \tfrac{1}{2}(d_{xx}^{FF} - d_{yy}^{FF}) \times \delta(|K-K'|,2)\}\delta(m_P, m_P')\delta(m_J + m_F, m_J' + m_F')(-1)^{\tau_{FF}}\tfrac{1}{2}(2J+1)\sqrt{15} \times \begin{pmatrix} J & 2 & J \\ -K & K-K' & K' \end{pmatrix} \begin{pmatrix} J & 2 & J \\ -m_J & m_J - m_J' & m_J' \end{pmatrix} \begin{pmatrix} I_F & 2 & I_F' \\ -m_F & m_F - m_F' & m_F' \end{pmatrix}$$

when $\tau_{FF} = \tau_F$ defined above. In these equations, it has nowhere been assumed that $I_P = \frac{1}{2}$, so that the results can be applied directly to cases where the single on-axis spin is larger than $\frac{1}{2}$.

The spin–rotation coupling constants are defined as the negatives of those derived by Flygare (34). The spin–spin constants can be expressed in a simple form if the electron-coupled contribution is dropped and if effects due to zero-point vibration and centrifugal distortion are neglected. The errors introduced should be small.

$$[A8a]\quad \tfrac{1}{2}(d_{yz}^{PF} + d_{zy}^{PF}) = \frac{3\mu_0\mu_N^2 g_P g_F}{4\pi R_{PF}^3}\sin\Theta_0\cos\Theta_0 \rightarrow -15.73\ \text{kHz}$$

$$[A8b] \quad \tfrac{1}{2}(d_{xx}^{PF} - d_{yy}^{PF}) = -\frac{3\mu_0\mu_N^2 g_P g_F}{8\pi R_{PF}^3}\sin^2\Theta_0 \qquad \rightarrow \quad 15.50\ \text{kHz}$$

$$[A8c] \quad \tfrac{1}{2}(d_{yz}^{FF} + d_{zy}^{FF}) = 0$$

$$[A8d] \quad \tfrac{1}{2}(d_{xx}^{FF} - d_{yy}^{FF}) = \frac{3\mu_0\mu_N^2 g_F^2}{16\pi R_{FF}^3} = \tfrac{3}{2}d^{FF} \qquad \rightarrow \quad 6.14\ \text{kHz}$$

Here R_{FF} and R_{PF} are the fluorine–fluorine and fluorine–phosphorus bond lengths, respectively. Θ_0 is the angle between the P—O and P—F bonds, corresponding to β in Fig. 1 of ref. 14; d^{FF} is given in [A8*d*]. The one remaining constant

$$[A8e] \quad d^{PF} = \frac{\mu_0\mu_N^2 g_P g_F}{4\pi R_{PF}^3}\cdot[1 - \tfrac{3}{2}\sin^2\Theta_0] \qquad \rightarrow -2.51\ \text{kHz}$$

The numerical values given in [A8] were obtained using the structure in ref. 11.